

## Article

## Intramolecular Energy and Electron Transfer Within a Diazaperopyrenium-Based Cyclophane

Xirui Gong, Ryan M. Young, Karel J. Hartlieb, Claire Miller, Yilei Wu, Hai Xiao,  
Peng Li, Nema Hafezi, Jiawang Zhou, Lin Ma, Tao Cheng, William A. Goddard,  
Omar K. Farha, Joseph T. Hupp, Michael R. Wasielewski, and J. Fraser Stoddart

*J. Am. Chem. Soc.*, **Just Accepted Manuscript** • DOI: 10.1021/jacs.6b13223 • Publication Date (Web): 22 Feb 2017

Downloaded from <http://pubs.acs.org> on February 24, 2017

### Just Accepted

“Just Accepted” manuscripts have been peer-reviewed and accepted for publication. They are posted online prior to technical editing, formatting for publication and author proofing. The American Chemical Society provides “Just Accepted” as a free service to the research community to expedite the dissemination of scientific material as soon as possible after acceptance. “Just Accepted” manuscripts appear in full in PDF format accompanied by an HTML abstract. “Just Accepted” manuscripts have been fully peer reviewed, but should not be considered the official version of record. They are accessible to all readers and citable by the Digital Object Identifier (DOI®). “Just Accepted” is an optional service offered to authors. Therefore, the “Just Accepted” Web site may not include all articles that will be published in the journal. After a manuscript is technically edited and formatted, it will be removed from the “Just Accepted” Web site and published as an ASAP article. Note that technical editing may introduce minor changes to the manuscript text and/or graphics which could affect content, and all legal disclaimers and ethical guidelines that apply to the journal pertain. ACS cannot be held responsible for errors or consequences arising from the use of information contained in these “Just Accepted” manuscripts.



ACS Publications



# Intramolecular Energy and Electron Transfer Within a Diazaperopyrenium-Based Cyclophane

Xirui Gong,<sup>#†</sup> Ryan M. Young,<sup>#†‡</sup> Karel J. Hartlieb,<sup>†</sup> Claire Miller,<sup>†‡</sup> Yilei Wu,<sup>†‡</sup> Hai Xiao,<sup>§</sup> Peng Li,<sup>†</sup> Nema Hafezi,<sup>†</sup> Jiawang Zhou,<sup>†‡</sup> Lin Ma,<sup>†‡</sup> Tao Cheng,<sup>§</sup> William A. Goddard, III<sup>§</sup>, Omar K. Farha,<sup>†||</sup>, Joseph T. Hupp,<sup>†</sup> Michael R. Wasielewski<sup>†‡\*</sup> and J. Fraser Stoddart<sup>†\*</sup>

<sup>†</sup>Department of Chemistry and <sup>‡</sup>Argonne-Northwestern Solar Energy Research (ANSER) center, Northwestern University, 2145 Sheridan Road, Evanston, Illinois 60208, United States

<sup>||</sup>Department of Chemistry, Faculty of Science, King Abdulaziz University, Jeddah 22254, Saudi Arabia

<sup>§</sup>Materials and Process Simulation Center, California Institute of Technology, Pasadena, California 91125, United States

<sup>#</sup>These authors contributed equally

\*E-mail: [stoddart@northwestern.edu](mailto:stoddart@northwestern.edu);  
[m-wasielewski@northwestern.edu](mailto:m-wasielewski@northwestern.edu)

## MAIN TEXT

**Abstract** Molecules capable of performing highly efficient energy transfer and ultrafast photo-induced electron transfer in well-defined multichromophoric structures are indispensable to the development of artificial photosynthetic systems. Herein, we report on the synthesis, characterization and photophysical properties of a rationally designed multichromophoric tetracationic cyclophane, **DAPPBox**<sup>4+</sup>, containing a diazaperopyrenium (DAPP<sup>2+</sup>) unit and an extended viologen (ExBIPY<sup>2+</sup>) unit, which are linked together by two *p*-xylylene bridges. Both <sup>1</sup>H NMR spectroscopy and single crystal X-ray diffraction analysis confirm the formation of an asymmetric, rigid, box-like cyclophane, **DAPPBox**<sup>4+</sup>. The solid-state superstructure of this cyclophane reveals a herringbone-type packing motif, leading to two types of  $\pi \cdots \pi$  interactions: (i) between the ExBIPY<sup>2+</sup> unit and the DAPP<sup>2+</sup> unit ( $\pi \cdots \pi$  distance of 3.7 Å) in the adjacent parallel cyclophane, as well as (ii) between the ExBIPY<sup>2+</sup> unit ( $\pi \cdots \pi$  distance of 3.2 Å) and phenylene ring in the closest orthogonal cyclophane. Moreover, the solution-phase photophysical properties of this cyclophane have been investigated by both steady-state and time-resolved absorption and emission spectroscopies. Upon photoexcitation of **DAPPBox**<sup>4+</sup> at 330 nm, rapid and quantitative intramolecular energy transfer occurs from the <sup>1</sup>\*ExBIPY<sup>2+</sup> unit to the DAPP<sup>2+</sup> unit in 0.5 ps to yield <sup>1</sup>\*DAPP<sup>2+</sup>. The same excitation wavelength simultaneously populates a higher excited state of <sup>1</sup>\*DAPP<sup>2+</sup> which then undergoes ultrafast intramolecular electron transfer from <sup>1</sup>\*DAPP<sup>2+</sup> to ExBIPY<sup>2+</sup> to yield the DAPP<sup>3+•</sup> – ExBIPY<sup>+•</sup> radical ion pair in  $\tau = 1.5$  ps. Selective excitation of DAPP<sup>2+</sup> at 505 nm populates a lower excited state where electron transfer is kinetically unfavorable.

## ■ INTRODUCTION

The construction of well-organized multi-chromophoric architectures, capable of performing efficient energy transfer (EnT) and electron transfer<sup>1</sup> (ET), is an indispensable part of the development of photofunctional systems. The key to the design of such synthetic systems is controlling the electronic interactions between donors (D) and acceptors (A) to optimize efficient energy transfer (EnT) and/or electron transfer (ET). Encouraging progress has been made on the construction of photofunctional systems, extending from discrete (1D) to extended (2D and 3D) structures, such as  $\pi$ -stacked molecules,<sup>2</sup> covalently linked porphyrin arrays,<sup>3</sup> dendrimers,<sup>4</sup> chromophoric polymers,<sup>5</sup> self-assembled structures,<sup>6</sup> and hybrid organic-inorganic structures.<sup>7</sup> Recently, the photophysical properties (either EnT or ET) of a newly synthesized tetracationic cyclophane, **ExBox**<sup>4+</sup>, and its supramolecular complexes have been investigated.<sup>8</sup> **ExBox**<sup>4+</sup> is related to cyclobis(paraquat-*p*-phenylene) wherein the 4,4'-bipyridinium units have been replaced with an extended *p*-phenylene-bridged bipyridinium unit, ExBIPY<sup>2+</sup>. Multi-electron accumulation<sup>7e</sup> and photo-induced charge shift reactions of **ExBox**<sup>4+</sup> have been demonstrated by intramolecular<sup>9</sup> through-bond electron transfer from the *p*-xylylene bridges to the extended bipyridinium units (ExBIPY<sup>2+</sup>) within **ExBox**<sup>4+</sup> itself as well as by intermolecular<sup>6c</sup> photo-induced charge shift within perylene $\subset$ **ExBox**<sup>4+</sup> complexes. On the other hand, EnT processes have been observed<sup>6e, 6f</sup> in supramolecular systems, by binding **ExBox**<sup>4+</sup> to other chromophores, like perylene-3,4:9,10-bis(dicarboximide)s (PDIs) (Figure 1a). Although one of the ExBIPY<sup>2+</sup> units in **ExBox**<sup>4+</sup> can undergo intramolecular photo-induced charge separation if excited with UV light, optimum utilization of the solar spectrum for artificial photosynthesis requires systems that absorb at wavelengths >400 nm. Given this requirement, we have designed an asymmetric cyclophane which incorporates one ExBIPY<sup>2+</sup> (Figure 1b) electron acceptor unit. For a second chromophore

1  
2  
3 to work alongside an ExBIPY<sup>2+</sup> unit within the geometry of a cyclophane molecule, that  
4  
5 chromophore must satisfy several criteria. First of all, the chromophore must be able to form a  
6  
7 donor-acceptor pair with an ExBIPY<sup>2+</sup> unit. Secondly, it should have a similar length as an  
8  
9 ExBIPY<sup>2+</sup> unit to ensure that the cyclophane retains its rectangular shape, which (i) promotes good  
10  
11 electronic coupling between the donor and acceptor in the face-to-face geometry as well as (ii)  
12  
13 provides an opportunity to bind guests, which may be used to modulate the coupling between the  
14  
15 donor and the acceptor; thereby allowing control over charge separation and recombination rates.<sup>6c</sup>  
16  
17  
18

19  
20 A class of molecules that match the above criteria are the diazaperopyrenium dications,<sup>10</sup>  
21  
22 shown in Figure 1c. Although these dications are structurally related, and share similar optical  
23  
24 properties to those of the PDIs, they possess enhanced solubility as a result of their dicationic  
25  
26 nature. Additionally, DAPP<sup>2+</sup> dications can be dissolved selectively either in organic solvents (soft  
27  
28 counterions, e.g., PF<sub>6</sub><sup>-</sup>, BF<sub>4</sub><sup>-</sup>) or in aqueous environments (hard counterions, e.g., CF<sub>3</sub>CO<sub>2</sub><sup>-</sup>, Cl<sup>-</sup>).  
29  
30 Since energy transfer between ExBIPY<sup>2+</sup> and PDI has been described<sup>6e, 6f</sup> in self-assembled  
31  
32 systems, we expect that, by incorporating a DAPP<sup>2+</sup> dicationic unit into a constitutionally  
33  
34 asymmetric cyclophane along with an ExBIPY<sup>2+</sup> unit, the unique arrangement of  
35  
36 multichromophoric units could demonstrate special photophysical properties, while avoiding  
37  
38 solubility issues commonly associated with PDIs.<sup>11</sup> The known properties<sup>10e</sup> of the DAPP<sup>2+</sup>  
39  
40 dication suggest these dicationic units as suitable substitutes for PDIs for incorporation into  
41  
42 multichromophoric cyclophanes.  
43  
44  
45  
46  
47

48  
49 Here, we report a rational design and preparation of a cyclophane, **DAPPBox**<sup>4+</sup> (Figure 1d),  
50  
51 containing one DAPP<sup>2+</sup> unit and one ExBIPY<sup>2+</sup> unit, which are bridged together by two *p*-xylylene  
52  
53 linkers. This constitutionally asymmetric tetracationic cyclophane is readily soluble in both  
54  
55 organic solvents, e.g., MeCN, MeNO<sub>2</sub> and DMF, as a PF<sub>6</sub><sup>-</sup> salt, and in water as a Cl<sup>-</sup> or TFA<sup>-</sup>  
56  
57  
58  
59  
60

salt. In this investigation, we have combined steady-state measurements, visible and near-infrared (NIR) transient absorption spectroscopy, and electronic structure calculations, in order to investigate the photophysical processes within **DAPPBox**<sup>4+</sup>. Our results show that photoexcitation of the ExBIPY<sup>2+</sup> electron acceptor within **DAPPBox**<sup>4+</sup> results in ultrafast energy transfer to the lowest excited state of the DAPP<sup>2+</sup> electron donor, followed by competitive fluorescence and intersystem crossing. Owing to the overlapping absorption of the subunits at 330 nm, excitation at this wavelength also leads to a small population of highly excited <sup>1</sup>\*DAPP<sup>2+</sup> which decays by electron transfer to DAPP<sup>3+</sup> – ExBIPY<sup>+</sup> in  $\tau = 1.5$  ps. Electron transfer from the lowest excited state of <sup>1</sup>\*DAPP<sup>2+</sup> around 2.46 eV is kinetically unfavorable in the cyclophane, leading to the same decay previously observed in DAPP<sup>2+</sup>. This rationally designed **DAPPBox**<sup>4+</sup> can perform both energy and electron transfer processes. The detailed study of the photophysical properties of the cyclophane constitutes an important fundamental step toward the understanding of competitive photophysical processes in the context of controlled molecular geometries.

## ■ RESULTS AND DISCUSSION

### Synthesis of the **DAPPBox**•4PF<sub>6</sub>

The synthesis of **DAPPBox**<sup>4+</sup> is outlined in Scheme 1. Briefly, S<sub>N</sub>2 reactions between an excess of 3,4,9,10-tetrakis(chloromethyl)perylene (**1**) and 4-(aminomethyl)benzenemethanol (**2**) in Me<sub>2</sub>SO at room temperature for 5 h, lead to the formation of **3**. Subsequently, **3** is oxidized by 2,3-dichloro-5,6-dicyano-1,4-benzoquinone (DDQ) in DMF at room temperature for 8 h to afford, after counterion exchange, **4**•2PF<sub>6</sub>. Bromination of **4**•2PF<sub>6</sub> with PBr<sub>3</sub> in MeCN at room temperature overnight, followed by counterion exchange with NH<sub>4</sub>PF<sub>6</sub>, results in the formation of the dibromide **BrDAPP**•2PF<sub>6</sub>. Finally, pyrene-templated<sup>8b</sup> cyclization between **BrDAPP**•2PF<sub>6</sub>

and 4,4'-(1,4-phenylene)bispyridine (ExBIPY) in MeCN at room temperature for 7 days, followed by precipitation of the crude product with tetrabutylammonium chloride (TBACl), gives pyrene $\subset$ **DAPPBox**•4Cl. This complex can then be dissolved in H<sub>2</sub>O and the aqueous solution subjected to continuous extraction with CHCl<sub>3</sub> for 3 days in order to remove the pyrene guest molecule from the cyclophane. The desired product **DAPPBox**•4PF<sub>6</sub> was isolated by reverse-phase column chromatography, followed by counterion exchange (NH<sub>4</sub>PF<sub>6</sub> / H<sub>2</sub>O) in 35% yield. The formation of **DAPPBox**•4PF<sub>6</sub> was confirmed by recording the <sup>1</sup>H NMR spectrum (Figure 2) in MeCN at room temperature. The peaks in the spectrum were assigned based on the analyses of two-dimensional <sup>1</sup>H-<sup>1</sup>H COSY NMR (Figure S1a) and 2D NOESY NMR (Figure S1b) spectra. As a result of its asymmetric constitution, two sets of peaks can be assigned to the methylene protons (H<sub>1</sub> / H<sub>2</sub>,  $\delta$  = 6.27 / 5.63 ppm) as well as another two sets of peaks to the phenylene protons (H<sub>Ar1</sub> / H<sub>Ar2</sub>,  $\delta$  = 7.87 / 7.59 ppm) of the *p*-xylylene linkers. High-resolution mass spectrometry (HRMS) revealed the presence of the [M – PF<sub>6</sub>]<sup>+</sup>, [M – 2PF<sub>6</sub>]<sup>2+</sup>, and [M – 3PF<sub>6</sub>]<sup>3+</sup> species which were detected at  $m/z$  = 1203.2074, 529.1266, and 304.4293, respectively.

Further evidence for cyclophane formation comes from single-crystal X-ray diffraction (XRD), Figure 3. Single crystals were grown by vapor diffusion of *i*-Pr<sub>2</sub>O into an MeCN solution of **DAPPBox**•4TFA during one week. The solid-state structure (Figure 3a) reveals an asymmetric, box-like cyclophane, with average dimensions of 14.1 by 7.1 Å (Figure 3b). The two torsional angles between the pyridinium and the *p*-phenylene rings are ~17° and ~20° (Figure 3c), respectively, i.e., they are smaller than the average torsional angle (~30°)<sup>8a</sup> in **ExBox**<sup>4+</sup>. This flatter conformation for the ExBIPY<sup>2+</sup> unit in **DAPPBox**<sup>4+</sup> is probably a consequence of intermolecular  $\pi\cdots\pi$  interactions<sup>12</sup> between the ExBIPY<sup>2+</sup> unit and adjacent cyclophanes. The *p*-xylylene ring in the closest adjacent cyclophane ( $\pi\cdots\pi$  distance of 3.2 Å) is associated with a torsional angle of

~17° in the ExBIPY<sup>2+</sup> unit, while the larger torsional angle (~20°) is adjacent to the relative weaker intermolecular aromatic recognition ( $\pi\cdots\pi$  distance of 3.7 Å) between the ExBIPY<sup>2+</sup> unit and the DAPP<sup>2+</sup> unit in another adjacent cyclophane. The perspective view of solid-state superstructure (Figure 3d) of **DAPPBox**<sup>4+</sup> reveals only partial  $\pi\cdots\pi$  overlap between the ExBIPY<sup>2+</sup> unit and a DAPP<sup>2+</sup> unit in a neighboring cyclophane, most likely arising from the balance between Coulombic repulsions and the maximization of  $\pi$ -overlap.<sup>10h</sup> The overall superstructure of **DAPPBox**<sup>4+</sup> reveals a herringbone type of packing.

The templating role played by pyrene during the synthesis of the cyclophane is supported by the solid-state superstructure (Figure S5) of the complex, pyrene  $\subset$  **DAPPBox**•4PF<sub>6</sub>. Single crystals, suitable for X-ray crystallography, were obtained by slow vapor diffusion of *i*Pr<sub>2</sub>O into a MeNO<sub>2</sub> solution of the complex. The superstructure reveals that pyrene sits inside the box at distances of 3.4 Å from the DAPP<sup>2+</sup> plane and 3.6 Å from the center of the ExBIPY<sup>2+</sup> unit. For full details, see the Supporting Information. In addition, the characteristic <sup>1</sup>H NMR signals of the macrocycle shift upon addition of pyrene (Figure S2), proving that complexation occurs between pyrene and **DAPPBox**<sup>4+</sup> in solution. A UV/Vis absorption-based Job plot (Figure S3b) confirms the 1:1 stoichiometry between **DAPPBox**<sup>4+</sup> and pyrene in MeCN, an observation which is in agreement with the solid-state superstructure. Furthermore, the fluorescence titration (Figure S3c) carried out upon the addition of pyrene into an MeCN solution of the **DAPPBox**<sup>4+</sup> (excitation at 440 nm) shows a decrease of **DAPP**<sup>2+</sup> fluorescence (515 nm), accompanied by a slight blue shift of the emission maxima, caused by either electronic perturbation or structural distortion upon host-



1  
2  
3 guest formation. Based on fluorescence titration data, the binding affinity  $K_a$  of complexation was  
4  
5  
6 calculated<sup>11b</sup> (Figure S3d) to be  $(3.73 \pm 0.35) \times 10^5 \text{ M}^{-1}$ .  
7

## 8 9 Reference Compound Absorption and Emission

10  
11 Two groups of reference compounds with methyl groups (Figure 4a) and benzyl groups (Figure  
12  
13 4b) attached to the nitrogen atoms in the 2 and 9 positions<sup>10h</sup> were investigated to understand the  
14  
15 basic photophysical processes involved in each chromophore. Based on the results obtained from  
16  
17 these reference compounds, we observed that the benzyl groups enable an ET deactivation  
18  
19 pathway, a feature which was not found to be present in the corresponding methylated reference  
20  
21 compound.<sup>9</sup> Thus, the photophysics of the methylated reference compounds (**Me-ExBIPY**<sup>2+</sup> and  
22  
23 **Me-DAPP**<sup>2+</sup>) were compared to that of **DAPPBox**<sup>4+</sup>, when 330 nm photons were used to excite  
24  
25 **ExBIPY**<sup>2+</sup>, while the photophysics of the benzylated reference compounds (**Bn-ExBIPY**<sup>2+</sup> and  
26  
27 **Bn-DAPP**<sup>2+</sup>) were compared to that of **DAPPBox**<sup>4+</sup>, when **DAPP**<sup>2+</sup> was selectively excited at 505  
28  
29 nm and 414 nm. Our data show that, in MeCN at room temperature, **Bn-ExBIPY**<sup>2+</sup> exhibits weak  
30  
31 UV fluorescence ( $\lambda_{\text{max}} = 378 \text{ nm}$ ,  $\Phi_{\text{fl}} = 3.8\%$ ), presumably as a result of deactivation by  
32  
33 photoinduced electron transfer from the benzyl rings to **ExBIPY**<sup>2+</sup>,<sup>9</sup> while strong UV emission is  
34  
35 observed ( $\lambda_{\text{max}} = 364 \text{ nm}$ ,  $\tau = 1.56 \text{ ns}$ ,  $\Phi_{\text{fl}} = 69\%$ , Figure S10) in the case of **Me-ExBIPY**<sup>2+</sup>, where  
36  
37 the electron transfer pathway is not present. Conversely, neither methyl nor benzyl substituents  
38  
39 significantly affect the **DAPP**<sup>2+</sup> behavior in either **Me-DAPP**<sup>2+</sup> ( $\lambda_{\text{max}} = 505 \text{ nm}$ ,  $\tau = 17.6 \text{ ns}$ ,  $\Phi_{\text{fl}} =$   
40  
41  $66\%$ , Figure S11) or **Bn-DAPP**<sup>2+</sup> ( $\lambda_{\text{max}} = 509 \text{ nm}$ ,  $\tau = 19.8 \text{ ns}$ ,  $\Phi_{\text{fl}} = 60\%$ , Figure S12), both of  
42  
43 which show strong green fluorescence, so electron transfer from these species is unlikely (*vide*  
44  
45 *infra*).  
46  
47  
48  
49  
50  
51  
52

53  
54 Some of the relevant photophysical data for all the compounds investigated are  
55  
56 summarized in Table 1, where the emission maxima refer to the spectra corrected for instrument  
57  
58  
59  
60

detection response. The UV/Vis absorption spectrum of the model compounds **Me-ExBIPY**<sup>2+</sup> and **Me-DAPP**<sup>2+</sup>, and the cyclophane **DAPPBox**<sup>4+</sup> recorded in MeCN are shown in Figure 5. The absorption bands for **Me-ExBIPY**<sup>2+</sup> occur at wavelengths shorter than 350 nm, with the maximum centered on 323 nm. The absorption spectrum for **Me-DAPP**<sup>2+</sup> is characterized by an intense band in the visible region, which is assigned to the  $S_2 \leftarrow S_0$  electronic transition ( $\lambda_{\text{max}} = 438$  nm), and in the UV region ( $< 325$  nm), assigned to the  $S_n \leftarrow S_0$  electronic transition ( $\lambda_{\text{max}} = 296$  nm). The exact ordering of the upper state accessed in this transition is left unassigned. The absorption of the **DAPPBox**<sup>4+</sup> exhibits minor differences when compared with the sum of the spectra of the corresponding model compounds, with only a slight red-shift of the absorption maximum ( $\lambda_{\text{max}} = 446$  nm). Importantly, from the reference compounds we see that at 330 nm, approximately 86% of the net extinction coefficient of **DAPPBox**<sup>4+</sup> can be assigned to the **ExBIPY**<sup>2+</sup> subunit, while the remaining 14% can be attributable to the **DAPP**<sup>2+</sup> absorption. Thus, we expect the excited states of each unit to participate in the dynamics following excitation.

## Excited State Dynamics

The excited state dynamics of **DAPPBox**<sup>4+</sup> and its subunits were probed by femtosecond and nanosecond transient absorption (fsTA/nsTA) spectroscopies. The fsTA spectra (Figures S15a and 18a) of both **Me-DAPP**<sup>2+</sup> and **Bn-DAPP**<sup>2+</sup>, following excitation at 330 nm, show similar spectral features: the ground state bleach appears at 505 nm overlapping with the singlet excited state absorption band, which spans from 450 to 900 nm and at 1440 nm. **Me-DAPP**<sup>2+</sup> and **Bn-DAPP**<sup>2+</sup> both show rapid internal conversion to a hot  $^*S_1$  state, followed by structural relaxation prior to decay of their singlet states (Figure S15a and S18a). The ~20 ns singlet state lifetimes for both **DAPP**<sup>2+</sup> derivatives are longer than the maximum pump-probe delay time (~8 ns) of the fsTA

experiment. The corresponding nsTA spectra (Figures S15b and S18b) show the  $^1\text{Me-DAPP}^{2+}$  and  $^1\text{Bn-DAPP}^{2+}$  singlet states decay to their respective triplet states with time constants similar to those observed by time-resolved fluorescence; the triplet states then decay back to the ground state in approximately 250 and 220 ns, respectively, in air-equilibrated solutions at room temperature, presumably by collisional triplet-triplet annihilation and/or oxygen quenching. The reasonably intense triplet signals are commensurate with the moderate fluorescence quantum yields for  $\text{Me-DAPP}^{2+}$  and  $\text{Bn-DAPP}^{2+}$ , as well as with the previous observation<sup>10c</sup> of the triplet state of  $\text{DAPP}^{2+}$ .

The transient absorption spectrum of  $\text{Bn-ExBIPY}^{2+}$  excited at 330 nm is shown in Figure S21.<sup>7e</sup> The spectrum is initially dominated by an intense peak at 495 nm, and a weaker feature around 1440 nm, which are assigned to the  $S_n \leftarrow S_1$  absorption. These features decay in  $\tau = 62 \pm 1$  ps as new bands peaking at 506 and 1110 nm appear. The spectra at this point strongly resemble  $\text{ExBIPY}^{+*}$ ,<sup>7e</sup> which confirms that fluorescence quenching of the  $^1\text{Bn-ExBIPY}^{2+}$  occurs by forward electron transfer. Back electron transfer occurs in 1200 ps, with some fraction recombining to the triplet state ( $T_n \leftarrow T_1$ , 480 nm).

The fsTA spectra of  $\text{DAPPBox}^{4+}$  following 330 nm excitation appear (Figure 6a) very similar in both  $\text{Me-DAPP}^{2+}$  and  $\text{Bn-DAPP}^{2+}$ . The absorption band present at ~1545 nm (Figure 6a) in the fsTA spectra of  $\text{DAPPBox}^{4+}$  persists for the entire singlet state lifetime (~20 ns), which is most likely the  $S_n \leftarrow S_1$  excited-state absorption of the  $\text{DAPP}^{2+}$  unit. The most noticeable difference is a pronounced, rapid decay of the absorption at 495 nm, and the appearance of a new absorption at 1150 nm. The 495 nm signal decays on a slower timescale, which is similar to that observed for the singlet decay of excited  $\text{DAPP}^{2+}$  chromophores. The 1150 nm band appears within the ~200 fs instrument response and exhibits multiple decay components. As in the  $\text{Me-DAPP}^{2+}$

and **Bn-DAPP**<sup>2+</sup> reference compounds, <sup>1</sup>\*DAPP<sup>2+</sup> decays to the triplet with an approximately 20 ns lifetime, and the triplet decays back to the ground state within 200 ns. Noticeably, the kinetics are more complicated in **DAPPBox**<sup>4+</sup> because of the overlapping ground state absorptions at the excitation wavelength (Figure 6).

To remove complications from the parallel excitations at 330 nm, we acquired the fsTA spectra of **DAPPBox**<sup>4+</sup> following excitation at 505 nm (Figure 6b), and separately at 414 nm (Figure S19). The spectra resemble those of both **Me-DAPP**<sup>2+</sup> and **Bn-DAPP**<sup>2+</sup>. Excitation at 414 nm again leads to rapid internal conversion to a hot <sup>\*</sup>S<sub>1</sub> state. There is a slower structural relaxation due to the rigid conformation of the box, followed by similar singlet state and triplet state lifetimes, 18 and 250 ns, respectively. Importantly, both the rapid decay of the peak at 495 nm and the new peak at 1150 nm that were observed when exciting at 330 nm are absent. This observation implies that exciting at lower photon energy shuts off some decay pathway(s), despite still exciting above the lowest energy excited state of DAPP<sup>2+</sup>.

### Efficient Energy Transfer within **DAPPBox**<sup>4+</sup>

We expect an available EnT decay pathway (Figure 7a) from comparison of the emission spectra ( $\lambda_{\text{exc}} = 554$  nm) in Figure 7b of **DAPPBox**<sup>4+</sup> with that of methylated reference compounds. Indeed, the emission spectrum of **DAPPBox**<sup>4+</sup> is devoid of UV fluorescence and is dominated by green emission ( $\tau = 19.5$  ns,  $\Phi_{\text{fl}} = 39\%$ , Figures S9) at 517 nm, even when the excitation occurs at ExBIPY<sup>2+</sup> absorption wavelengths ( $\lambda_{\text{exc}} = 339$  nm). The quenching of ExBIPY<sup>2+</sup> fluorescence at 380 nm, accompanied by the enhancement of the DAPP<sup>2+</sup> unit emission at 510 nm in the steady-state emission spectrum of **DAPPBox**<sup>4+</sup>, suggests efficient singlet EnT from the ExBIPY<sup>2+</sup> to the DAPP<sup>2+</sup> unit within the cyclophane. Such relative quenching and enhancement were not observed

in an equimolar physical mixture of **Me-ExBIPY**<sup>2+</sup> and **Me-DAPP**<sup>2+</sup>, indicating efficient EnT processes only occur within the cyclophane. This result can be rationalized by consideration of the conformation of the cyclophane which imparts (i) a reasonable spatial separation (7.1 Å, measured from single crystal structure, Figure 2b) between the energy donor (**ExBIPY**<sup>2+</sup>) and acceptor (**DAPP**<sup>2+</sup>) in **DAPPBox**<sup>4+</sup>, (ii) a face-to-face chromophore arrangement that aligns the transition dipole moments, and (iii) rigidity that limits conformational flexibility. The high efficiency of EnT is also in line with the favorable overlap (Figure 7c) of the emission spectra of **Me-ExBIPY**<sup>2+</sup> and the absorption spectra of **Me-DAPP**<sup>2+</sup>, as required for Förster energy transfer. Moreover, the almost perfect matching of the fluorescence excitation spectrum ( $\lambda_{em} = 554$  nm) and the UV/Vis absorption spectrum (Figure 7d) of **DAPPBox**<sup>4+</sup>, once again, corroborates the assignment of EnT process within **DAPPBox**<sup>4+</sup>.

The fsTA spectra support the observation of efficient energy transfer from <sup>1</sup>\***ExBIPY**<sup>2+</sup> to **DAPP**<sup>2+</sup> deduced from the fluorescence data. The fsTA spectra of **DAPPBox**<sup>4+</sup> following 330 nm excitation show (Figure 6a) increased intensity of the absorption band at 495 nm during the first few ps after excitation compared to those of **Bn-DAPP**<sup>2+</sup> (Figure S18a), and **DAPPBox**<sup>4+</sup> following 414 nm excitation (Figure S19a), suggesting the brief appearance of the locally excited state <sup>1</sup>\***ExBIPY**<sup>2+</sup> (Figure S21a). This relative enhancement does not appear in the spectra of **Me-DAPP**<sup>2+</sup> (Figure S15a) or **Bn-DAPP**<sup>2+</sup> (Figure S18a) nor does it appear in the spectra of **DAPPBox**<sup>4+</sup> when only the **DAPP**<sup>2+</sup> unit is excited (Figures 6b and S19a). Figure 8a shows a comparison of the kinetics at 495 nm for **DAPPBox**<sup>4+</sup> with **Me-ExBIPY**<sup>2+</sup> and **Me-DAPP**<sup>2+</sup> under identical conditions, while Figure 8b shows for the kinetic fits for **DAPPBox**<sup>4+</sup> when the **ExBIPY**<sup>2+</sup> and **DAPP**<sup>2+</sup> units are excited at 330 nm and 414 nm, respectively. Scatter of the 505 nm pump prevented the use of that dataset for this comparison. Upon fitting the kinetic decay at 495 nm, we

determined that the energy transfer occurs with a 0.5 ps time constant, which shows that energy transfer from  $^1\text{ExBIPY}^{2+}$  to  $\text{DAPP}^{2+}$  is highly efficient and outcompetes other deactivation pathways previously observed<sup>9</sup> in **ExBox**<sup>4+</sup>.

The rate of resonance EnT can be calculated using Förster theory based on the spectral overlap between the absorption of the **Me-ExBIPY**<sup>2+</sup> acceptor and the emission of the **Me-DAPP**<sup>2+</sup> donor. We have calculated the Förster EnT rate with the PhotochemCAD software package,<sup>19</sup> using the steady-state spectra, the fluorescence quantum yield of the donor, the distance between the donor and acceptor from the XRD data,<sup>13</sup> and the refractive index of the MeCN as inputs. The fixed parallel orientation of the donor and acceptor units in **DAPPBox**<sup>4+</sup> leads to an orientation factor of  $\kappa^2 = 1$ , as opposed to the typical value of  $\kappa^2 = 2/3$  for freely rotating molecules where re-orientation occurs faster than the emission timescale. The calculated EnT rate is therefore  $k_{\text{EnT}} = (0.43 \text{ ps})^{-1}$ , a value which is in excellent agreement with the experimental result of  $k_{\text{EnT}} = (0.5 \text{ ps})^{-1}$  and supports the Förster mechanism. Dexter energy transfer cannot be entirely ruled out, however, since there may be sufficient electronic wavefunction overlap between the donor and acceptor units to enable ultrafast electron transfer (*vide infra*).

Computational modeling of  $^1\text{DAPPBox}^{4+}$  using time-dependent density functional theory (TDDFT) predicts the first two major absorption peaks at 451 and 352 nm, which correspond to  $^1\text{DAPP}^{2+}$  and  $^1\text{ExBIPY}^{2+}$ , respectively, in good agreement with experimental observations. The electronic configuration of  $^1\text{ExBIPY}^{2+}$  is mainly composed of contributions from molecular orbitals (MOs) of the  $\text{ExBIPY}^{2+}$  unit, while the 451 nm excitation of the  $\text{DAPP}^{2+}$  unit involves (Figure S41) contributions from the MOs of the *p*-xylylene linkers and the  $\text{DAPP}^{2+}$  unit. The total quantum yield from emission of the **DAPPBox**<sup>4+</sup> can be calculated through the product of (i) the EnT efficiency of **DAPPBox**<sup>4+</sup> (98%, based on competing rates of the  $\text{ExBIPY}^{2+}$  excited-state

lifetime of 1.56 ns, and the **Bn-ExBIPY**<sup>2+</sup> charge transfer time of 60 ps), (ii) the photon absorption efficiency of **ExBIPY**<sup>2+</sup> at 330 nm (84%, based on extinction coefficients), and (iii) the fluorescence quantum yield of **Bn-DAPP**<sup>2+</sup> (0.66, excited at 375 nm). The calculated quantum yield of 0.54 ( $= 0.98 \times 0.84 \times 0.66$ ), for the cyclophane is slightly higher than the corresponding measured fluorescence quantum yield of 0.39. The difference between the calculated and experimental results can be explained by the difference between the quantum yields of the units in the cyclophane and those of the **ExBIPY**<sup>2+</sup> and **DAPP**<sup>2+</sup> reference compounds. Other possible means whereby the quantum yield of the cyclophane is decreased may arise from alternative decay pathways, e.g., an increased rate of internal conversion. We, however, have no direct evidence for any other competitive process.

### Ultrafast Electron Transfer within **DAPPBox**<sup>4+</sup>

The overlapping **DAPP**<sup>2+</sup> unit absorption at 330 nm leads to parallel excited state populations of <sup>1</sup>\***ExBIPY**<sup>2+</sup> and <sup>1</sup>\***DAPP**<sup>2+</sup> within **DAPPBox**<sup>4+</sup>, with the majority of the excitation on the **ExBIPY** moiety. With the observation of ultrafast energy transfer, we expect no significant yield of charge transfer from the *p*-xylylene linker to <sup>1</sup>\***ExBIPY**<sup>2+</sup> in the **DAPPBox**<sup>4+</sup> cyclophane, since this electron transfer occurs with a 60 ps time constant in **Bn-ExBIPY**<sup>2+</sup> and 240 ps in the **ExBox**<sup>4+</sup> cyclophane. We also do not observe any of the characteristic absorption bands<sup>10c</sup> for **DAPP**<sup>+</sup>, indicating that <sup>1</sup>\***ExBIPY**<sup>2+</sup> does not reduce the **DAPP**<sup>2+</sup> moiety within **DAPPBox**<sup>4+</sup>. If either of these charge transfer pathways were significant, the fluorescence quantum yield and lifetime of the cyclophane would be substantially lower.<sup>10c</sup>

However, the appearance of the 1150 nm band that is similar to the characteristic<sup>14, 6c, 9</sup> of **ExBIPY**<sup>+</sup> absorption alongside the **DAPP** suggests that the smaller of these populations decays by

ultrafast electron transfer. The red-shift of that band may arise due to Stark effects of the  $\text{DAPP}^{2+}$  moiety in close proximity. The 1150 nm band appears immediately following excitation and rises over the next few picoseconds. The fit of the **DAPPBox** $^{4+}$  spectra (Figure S37) indicates that the forward electron transfer from  $1^*\text{DAPP}^{2+}$  to  $\text{ExBIPY}^{2+}$  occurs in  $\tau_{\text{FET}} = 1.5$  ps. Therefore, we rule out transfer from the p-xylyl linker to  $\text{ExBIPY}$  (vide supra). Back electron transfer then follows in  $\tau_{\text{BET}} = 3.2 \pm 0.8$  ns. The back electron transfer time from the global fits of the fsTA data is consistent with the  $\tau = 2.2 \pm 1.2$  ns decay observed in the nsTA data (Figure S40). Additionally, as discussed above, no evidence for electron transfer from the p-xylyl linker to  $\text{DAPP}^{2+}$  was observed in the **Bn-DAPP** $^{2+}$  reference compound, suggesting that the 1150 nm absorption originates from the  $\text{DAPP}^{3+\bullet} - \text{ExBIPY}^{+\bullet}$  radical ion pair.

It should be noted that there is an absorption band present at 1520 nm. However, this band is not an indicator of electron transfer but rather is characteristic of the  $S_1$  state for **Bn-DAPP** $^{2+}$  (Figure S19) as a result of the 505 nm excitation, since (i) this 1520 nm absorption band in the NIR persists for the entire singlet lifetime ( $\sim 20$  ns as confirmed by time-resolved fluorescence) in the case of both **Bn-DAPP** $^{2+}$  (Figure S19) and **DAPPBox** $^{4+}$  (Figure 6b) when excited at 505 nm; and (ii) this band is also similar to the 1430 nm absorption band for **Me-DAPP** $^{2+}$  (no electron transfer possible when excited at 505 nm), shifted, however, by  $\sim 50$  meV ( $\sim 400$   $\text{cm}^{-1}$ ). The red shift of the band wavelength can be explained by substituent effects.

The excitation wavelength dependence of the fsTA signal indicates that electron transfer originates from a higher excited state of  $\text{DAPP}^{2+}$ . The cyclic voltammogram in Figure S7 shows that the oxidation potential of  $\text{DAPP}^{2+}$  in MeCN is 1.69 V vs. Ag/AgCl, while the reduction potential of  $\text{ExBIPY}^{2+}$  has been reported previously as -0.65 V vs Ag/AgCl.<sup>8a</sup> Using the Weller equation, we can estimate the energy of the  $\text{DAPP}^{3+\bullet} - \text{ExBIPY}^{+\bullet}$  radical ion pair state in MeCN as



$\Delta G_{IP} \approx E_{ox} - E_{red} = 2.34$  eV, and the free energy of photoinduced electron transfer from the various accessible excited states with singlet energy  $E_S$  is  $\Delta G_{ET} \approx \Delta G_{IP} - E_S$ . From this estimate, we see that electron transfer from  $S_1$  of DAPP<sup>2+</sup> at 2.46 eV is only slightly thermodynamically favorable. However, the solvent reorganization energy is around  $\sim 1$  eV in this solvent,<sup>6f</sup> Marcus theory predicts that the ET rate should be relatively slow. It is worth noting that the ion pair energy obtained from the Weller equation is likely an overly simplistic approximation. From DFT (see SI for details), we calculate the lowest energy ion-pair state to be around 2.47 eV; the  $\sim +0.13$  eV difference from the Weller estimate is enough to make ET from the DAPP<sup>2+</sup>  $S_1$  state thermodynamically unfavorable.

Interestingly, no ET is observed when exciting to the next higher energy excited state at 505 nm ( $S_1 \leftarrow S_0$  transition), or even 414 nm (higher vibronic band of the  $\sim 2.85$  eV  $S_2 \leftarrow S_0$  transition), even though  $\Delta G_{ET}$  is more negative. It is likely that the rate of internal conversion between the  $S_2$  and  $S_1$  states ( $\Delta E_S = -0.40$  eV) is substantially faster than that of ET, effectively shutting off the latter process. Thus we rule out ET from the lower energy excited states of DAPP<sup>2+</sup> as major sources of the ion pair population.

Only when exciting at 330 nm (3.76 eV) do we observe the radical ion pair absorption, implying that ET is at least competitive with other decay pathways and is perhaps the dominant process from this state. From the energy gap law for non-radiative decay processes, we expect internal conversion from this state ( $S_n$ ) to the lower lying  $S_2$  state (with gap  $\Delta E_S = -0.91$  eV) to be slower than that from  $S_2$  to  $S_1$ . At the same time, Marcus theory predicts that with  $\Delta G_{ET} \approx -1.41$  eV ( $-1.38$  eV using the DFT ion pair energy), the ET rate from the vertically prepared  $S_n$  state will be much closer to the top of the Marcus rate vs. free energy curve, and faster than that for ET from  $S_2$  or  $S_1$ . Thus the combination of faster ET and slower IC processes leads measurable population

of the ion pair state when exciting at 330 nm; the slower internal conversion from  $S_n$  serves as a minor “bottleneck” for relaxation, allowing ET to proceed. The excited state dynamics of **DAPPBox**<sup>4+</sup> at each excitation wavelength are summarized in Figure 9.

## ■ CONCLUSION

We report the stepwise synthesis of a rationally designed multichromophoric donor-acceptor cyclophane, **DAPPBox**<sup>4+</sup>. We demonstrate that the use of pyrene as a template favors the formation of this constitutionally asymmetric cyclophane in 35% yield. The structure of **DAPPBox**<sup>4+</sup> was determined by <sup>1</sup>H NMR spectroscopy, high resolution mass spectrometry in solution, and single crystal X-ray diffraction analysis in the solid state. Investigations carried out on the photophysical properties of the cyclophane excited at 330 nm by means of steady-state as well as time-resolved absorption and emission spectroscopies reveal, not only efficient energy transfer from the <sup>1</sup>\*ExBIPY<sup>2+</sup> to the DAPP<sup>2+</sup> unit in  $\tau = 0.5$  ps, but also the existence of an efficient, ultrafast intramolecular electron-transfer pathway: <sup>\*</sup>DAPP<sup>2+</sup>–ExBIPY<sup>2+</sup>  $\rightarrow$  DAPP<sup>3+</sup>–ExBIPY<sup>•+</sup> radical ion pair in  $\tau = 1.5$  ps. The photophysical investigations were also supported by TDDFT results. This class of constitutionally asymmetric cyclophanes may have considerable potential for integration into solar energy conversion and organic electronics. In the context of artificial photosynthesis, the next logical step towards utilizing **DAPPBox**<sup>4+</sup> will be to bind different guest molecules inside the cyclophane, forming 1:1 complexes, which can serve to modulate the electron transfer rates.

## ■ EXPERIMENTAL SECTION

**3:** 3,4,9,10-Tetrakis(chloromethyl)perylene<sup>15</sup> (**2**) (623 mg, 4.53 mmol) was added with stirring to a solution of 4-(aminomethyl)benzenemethanol<sup>16</sup> (**1**) (135 mg, 0.302 mmol) in Me<sub>2</sub>SO (8 mL) at room temperature. After 5 h, deionized H<sub>2</sub>O (100 mL) was added to the reaction mixture, forming

a dark yellow precipitate, which was filtered off, washed with deionized H<sub>2</sub>O and a small amount of EtOH, before being dried under vacuum to afford (147 mg, 85 %) a dark yellow solid **3**. The product was used without further purification in the next step. <sup>1</sup>H NMR (500 MHz, CD<sub>3</sub>SOCD<sub>3</sub>): δ<sub>H</sub> = 8.20 (d, *J* = 7.7 Hz, 4H), 7.32 (q, *J* = 8.0 Hz, 8H), 7.24 (d, *J* = 7.7 Hz, 4H), 4.50 (d, *J* = 5.7 Hz, 4H), 3.86 (s, 8H), 3.75 (s, 4H). <sup>13</sup>C NMR (126 MHz, CD<sub>3</sub>SOCD<sub>3</sub>): δ<sub>C</sub> = 140.8, 135.7, 132.7, 128.1, 125.1, 122.6, 119.1, 62.1, 60.3, 55.2. More detailed discussion of this reaction is available in the SI.

**4•2PF<sub>6</sub>**: DDQ (240 mg, 1.057 mmol) was added to a dark yellow solution of **3** (100 mg, 0.182 mmol) in DMF (8 mL) at room temperature. The color of the reaction mixture became dark brown upon the addition of the DDQ. After stirring for 8 h, a satd aqueous solution (100 mL) of NH<sub>4</sub>PF<sub>6</sub> was added to the reaction mixture. The resulting precipitate was filtered off, washed with deionized H<sub>2</sub>O and a small amount of EtOH, before being dried under vacuum to afford (138 mg, 90 %) a dark brown solid **4•2PF<sub>6</sub>**. The crude product was dissolved in MeCN in order to exchange the anions from PF<sub>6</sub><sup>-</sup> to Cl<sup>-</sup> by addition of an excess of tetrabutylammonium chloride (TBACl). The crude dibromide was then subjected to reverse-phase HPLC, starting with H<sub>2</sub>O / 0.1 % TFA as eluent and adding up to 100 % of MeCN / 0.1 % TFA to the eluent within 40 min. The pure fractions were collected and concentrated under vacuum. The residue was dissolved in H<sub>2</sub>O, followed by the addition of NH<sub>4</sub>PF<sub>6</sub> to yield pure **4•2PF<sub>6</sub>** (124 mg, 80 %). <sup>1</sup>H NMR (500 MHz, CD<sub>3</sub>SOCD<sub>3</sub>): δ<sub>H</sub> = 10.39 (s, 4H), 9.94 (s, 4H), 8.95 (s, 4H), 7.72 (d, *J* = 7.9 Hz, 4H), 7.45 (d, *J* = 7.8 Hz, 4H), 6.41 (s, 4H), 4.53 (s, 4H). <sup>13</sup>C NMR (126 MHz, CD<sub>3</sub>SOCD<sub>3</sub>): δ<sub>C</sub> = 150.4, 138.4, 128.3, 128.3, 126.5, 126.2, 113.7, 100.3, 61.8.

**BrDAPP•2PF<sub>6</sub>**: **4•2PF<sub>6</sub>** (100 mg, 0.116 mmol) was dissolved in MeCN (15 mL) and PBr<sub>3</sub> (100 μL, 1.063 mmol) was added slowly while stirring at room temperature overnight. A satd aqueous solution (100 mL) of NH<sub>4</sub>PF<sub>6</sub> was added to quench the reaction, resulting in the formation of a reddish brown solid. The resulting precipitate was filtered off, washed with deionized H<sub>2</sub>O and a small amount of EtOH, before being dried under vacuum to afford (80 mg, 70 %) a reddish brown solid **BrDAPP•2PF<sub>6</sub>**. <sup>1</sup>H NMR (500 MHz, CD<sub>3</sub>SOCD<sub>3</sub>): δ<sub>H</sub> = 10.44 (s, 4H), 10.04 (d, *J* = 9.6 Hz, 4H), 9.04 (d, *J* = 9.3 Hz, 4H), 7.72 (d, *J* = 7.9 Hz, 4H), 7.60 (d, *J* = 8.0 Hz, 4H), 6.45 (s, 4H), 4.74 (s, 4H). <sup>13</sup>C NMR (126 MHz, CD<sub>3</sub>SOCD<sub>3</sub>): δ<sub>C</sub> = 161.7, 138.8, 129.5, 128.7, 127.7, 127.2, 126.1, 63.7, 39.0, 33.0.

**DAPPBox•4PF<sub>6</sub>**: A solution of **BrDAPP•2PF<sub>6</sub>** (1 equiv), ExBIPY (1 equiv) and pyrene (6 equiv) in dry MeCN was stirred at room temperature for 7 days. Excess of TBACl was added to quench the reaction and the resulting crude precipitate was then dissolved in H<sub>2</sub>O and the pyrene template was removed by continuous liquid-liquid extraction with CHCl<sub>3</sub> and H<sub>2</sub>O over 3 days. The aqueous phase was concentrated to a small volume and then subjected to reverse-phase HPLC, starting with H<sub>2</sub>O / 0.1 % TFA as eluent, and adding up to 100 % of MeCN / 0.1% TFA as eluent within 45 min. The pure fractions were collected and concentrated in vacuum. The residue was dissolved in H<sub>2</sub>O, followed by the addition of NH<sub>4</sub>PF<sub>6</sub> to afford pure **DAPPBox•4PF<sub>6</sub>** in 35 % yield. <sup>1</sup>H NMR (500 MHz, CD<sub>3</sub>CN): δ<sub>H</sub> = 9.96 (s, 4H), 9.65 (s, 4H), 8.86 (s, 4H), 8.65 (d, *J* = 6.1 Hz, 4H), 7.95 – 7.83 (m, 8H), 7.61 (d, *J* = 8.0 Hz, 4H), 7.54 (s, 4H), 6.28 (s, 4H), 5.62 (s, 4H). <sup>13</sup>C NMR (126 MHz, CD<sub>3</sub>CN): δ<sub>C</sub> = 144.5, 138.2, 130.8, 130.6, 129.3, 127.0, 126.0, 66.4, 64.5. HRMS (ESI) for **DAPPBox•4PF<sub>6</sub>**; Calcd for C<sub>56</sub>H<sub>40</sub>F<sub>24</sub>N<sub>4</sub>P<sub>4</sub>: *m/z* = 1203.2174 [*M* – PF<sub>6</sub>]<sup>+</sup>; Found : 1203.2173 [*M* – PF<sub>6</sub>]<sup>+</sup>; 529.1266 [*M* – 2PF<sub>6</sub>]<sup>2+</sup>; Found : 529.1263 [*M* – 2PF<sub>6</sub>]<sup>2+</sup>; 304.4293 [*M* – 3PF<sub>6</sub>]<sup>3+</sup>; Found : 304.4293 [*M* – 3PF<sub>6</sub>]<sup>3+</sup>.

## Single-Crystal X-ray Diffraction (XRD)

**DAPPBox•4TFA.** (a) *Method.* A 0.25mM MeCN solution of **DAPPBox•4TFA** was filtered through a 0.45- $\mu$ m syringe filter into VWR culture tubes. The culture tubes were placed in one closed 20-mL scintillation vial containing 3 mL *i*Pr<sub>2</sub>O. After 7 days, reddish brown crystals of **DAPPBox•4TFA** were obtained. A suitable crystal was selected and mounted in inert oil and transferred to the cold gas stream of a Bruker Kappa APEX CCD area detector diffractometer. The crystal was kept at 100 K during data collection. Using Olex2,<sup>17</sup> the structure was solved with the XM<sup>18</sup> structure solution program using Dual Space and refined with the XL refinement package using Least Squares minimization. (b) *Crystal Parameters.* **DAPPBox•4TFA**, orange needles,  $M = 2442.00$ , crystal size  $0.124 \times 0.122 \times 0.02$  mm<sup>3</sup>, triclinic, space group  $P\bar{1}$ ,  $a = 13.3141(7)$ ,  $b = 21.1146(10)$ ,  $c = 23.4964(13)$  Å,  $\alpha = 96.654(4)$ ,  $\beta = 99.661(4)$ ,  $\gamma = 105.932(4)^\circ$ ,  $V = 6169.5(6)$  Å<sup>3</sup>,  $\rho_{calc} = 1.315$ ,  $T = 100$  K,  $Z = 2$ ,  $R_1(F^2 > 2\sigma F^2) = 0.0982$ ,  $\omega R_2 = 0.2196$ . Out of 26407 reflections a total of 25028 were unique. Crystallographic data (excluding structure factors) for the structures reported in this communication have been deposited with the Cambridge Crystallographic Data Center as supplementary publication nos. CCDC – 1480961.

## ■ ACKNOWLEDGEMENTS

This research was conducted as part of the Joint Center of Excellence in Integrated Nanosystems at King Abdulaziz City for Science and Technology (KACST) and Northwestern University (NU). The authors thank both KACST and NU for their continued support of this research. This work was also supported by the Chemical Sciences, Geosciences, and Biosciences Division, Office of Basic Energy Sciences, US DOE under grant no. DE-FG02-99ER14999 (M.R.W.). J.T.H. and O.K.F. gratefully acknowledge financial support by the U. S. Department of Energy, Office of Science, Office of Basic Energy Sciences (grant No. DE-FG02 87ER13808) and Northwestern University.

## ■ ASSOCIATED CONTENT

### Supporting Information

Experimental detail, including synthesis, NMR, UV-Vis-NIR, fluorescence emission and excitation, fsTA data, and electrochemical experiments, are available in the Supporting Information. This material is available free of charge via the Internet at <http://pubs.acs.org>.

## ■ REFERENCES

- (a) Brédas, J.-L.; Beljonne, D.; Coropceanu, V.; Cornil, J. *Chem. Rev.* **2004**, *104*, 4971. (b) Kirner, S.; Sekita, M.; Guldi, D. M. *Adv. Mater.* **2014**, *26*, 1482.
- (a) Vura-Weis, J.; Abdelwahed, S. H.; Shukla, R.; Rathore, R.; Ratner, M. A.; Wasielewski, M. R. *Science* **2010**, *328*, 1547. (b) Goransson, E.; Emanuelsson, R.; Jorner, K.; Markle, T. F.; Hammarstrom, L.; Ottosson, H. *Chem. Sci.* **2013**, *4*, 3522. (c) Strauss, V.; Margraf, J. T.; Dirian, K.; Syrgiannis, Z.; Prato, M.; Wessendorf, C.; Hirsch, A.; Clark, T.; Guldi, D. M. *Angew. Chem., Int. Ed.* **2015**, *54*, 8292.
- (a) Aratani, N.; Kim, D.; Osuka, A. *Acc. Chem. Res.* **2009**, *42*, 1922. (b) Patwardhan, S.; Sengupta, S.; Siebbeles, L. D. A.; Würthner, F.; Grozema, F. C. *J. Am. Chem. Soc.* **2012**, *134*, 16147. (c) Parkinson, P.; Knappke, C. E. I.; Kamonsutthipaijit, N.; Sirithip, K.; Matichak, J. D.; Anderson, H. L.; Herz, L. M. *J. Am. Chem. Soc.* **2014**, *136*, 8217. (d) Ragoussi, M.-E.; Katsukis, G.; Roth, A.; Malig, J.; de la Torre, G.; Guldi, D. M.; Torres, T. *J. Am. Chem. Soc.* **2014**, *136*, 4593. (e) Sukegawa, J.; Schubert, C.; Zhu, X.; Tsuji, H.; Guldi, D. M.; Nakamura, E. *Nature Chem.* **2014**, *6*, 899. (f) Rousseaux, S. A. L.; Gong, J. Q.; Haver, R.; Odell, B.; Claridge, T. D. W.; Herz, L. M.; Anderson, H. L. *J. Am. Chem. Soc.* **2015**, *137*, 12713. (g) Tanaka, T.; Osuka, A. *Chem. Soc. Rev.* **2015**, *44*, 943. (h) Antoniuk-Pablant, A.; Kodis, G.; Moore, A. L.; Moore, T. A.; Gust, D. *J. Phys. Chem. B* **2016**, *120*, 6687.
- Galindo, J. F.; Atas, E.; Altan, A.; Kuroda, D. G.; Fernandez-Alberti, S.; Tretiak, S.; Roitberg, A. E.; Kleiman, V. D. *J. Am. Chem. Soc.* **2015**, *137*, 11637.
- Ricks, A. B.; Brown, K. E.; Wenninger, M.; Karlen, S. D.; Berlin, Y. A.; Co, D. T.; Wasielewski, M. R. *J. Am. Chem. Soc.* **2012**, *134*, 4581.
- (a) Schmidt-Mende, L.; Fechtenkötter, A.; Müllen, K.; Moons, E.; Friend, R. H.; MacKenzie, J. D. *Science* **2001**, *293*, 1119. (b) Gunderson, V. L.; Smeigh, A. L.; Kim, C. H.; Co, D. T.; Wasielewski, M. R. *J. Am. Chem. Soc.* **2012**, *134*, 4363. (c) Young, R. M.; Dyar, S. M.; Barnes, J. C.; Juriček, M.; Stoddart, J. F.; Co, D. T.; Wasielewski, M. R. *J.*

- Phys. Chem. A* **2013**, *117*, 12438. (d) Gallego, M.; Calbo, J.; Aragón, J.; Krick Calderon, R. M.; Liquido, F. H.; Iwamoto, T.; Greene, A. K.; Jackson, E. A.; Pérez, E. M.; Ortí, E.; Guldi, D. M.; Scott, L. T.; Martín, N. *Angew. Chem., Int. Ed.* **2014**, *53*, 2170. (e) Ryan, S. T. J.; Del Barrio, J.; Ghosh, I.; Biedermann, F.; Lazar, A. I.; Lan, Y.; Coulston, R. J.; Nau, W. M.; Scherman, O. A. *J. Am. Chem. Soc.* **2014**, *136*, 9053. (f) Ryan, S. T. J.; Young, R. M.; Henkelis, J. J.; Hafezi, N.; Vermeulen, N. A.; Hennig, A.; Dale, E. J.; Wu, Y.; Krzyaniak, M. D.; Fox, A.; Nau, W. M.; Wasielewski, M. R.; Stoddart, J. F.; Scherman, O. A. *J. Am. Chem. Soc.* **2015**, *137*, 15299.
7. (a) Lee, C. Y.; Farha, O. K.; Hong, B. J.; Sarjeant, A. A.; Nguyen, S. T.; Hupp, J. T. *J. Am. Chem. Soc.* **2011**, *133*, 15858. (b) Oelsner, C.; Herrero, M. A.; Ehli, C.; Prato, M.; Guldi, D. M. *J. Am. Chem. Soc.* **2011**, *133*, 18696. (c) Jin, S.; Son, H.-J.; Farha, O. K.; Wiederrecht, G. P.; Hupp, J. T. *J. Am. Chem. Soc.* **2013**, *135*, 955. (d) Son, H.-J.; Jin, S.; Patwardhan, S.; Wezenberg, S. J.; Jeong, N. C.; So, M.; Wilmer, C. E.; Sarjeant, A. A.; Schatz, G. C.; Snurr, R. Q.; Farha, O. K.; Wiederrecht, G. P.; Hupp, J. T. *J. Am. Chem. Soc.* **2013**, *135*, 862. (e) Young, R. M.; Jensen, S. C.; Edme, K.; Wu, Y.; Krzyaniak, M. D.; Vermeulen, N. A.; Dale, E. J.; Stoddart, J. F.; Weiss, E. A.; Wasielewski, M. R.; Co, D. T. *J. Am. Chem. Soc.* **2016**, *138*, 6163.
8. (a) Barnes, J. C.; Juriček, M.; Strutt, N. L.; Frascioni, M.; Sampath, S.; Giesener, M. A.; McGrier, P. L.; Bruns, C. J.; Stern, C. L.; Sarjeant, A. A.; Stoddart, J. F. *J. Am. Chem. Soc.* **2013**, *135*, 183. (b) Barnes, J. C.; Juriček, M.; Vermeulen, N. A.; Dale, E. J.; Stoddart, J. F. *J. Org. Chem.* **2013**, *78*, 11962. (c) Dale, E. J.; Vermeulen, N. A.; Juriček, M.; Barnes, J. C.; Young, R. M.; Wasielewski, M. R.; Stoddart, J. F. *Acc. Chem. Res.* **2016**, *49*, 262.
9. Dyar, S. M.; Barnes, J. C.; Juriček, M.; Stoddart, J. F.; Co, D. T.; Young, R. M.; Wasielewski, M. R. *Angew. Chem., Int. Ed.* **2014**, *53*, 5371.
10. (a) Slama-Schwok, A.; Jazwinski, J.; Béré, A.; Montenay-Garestier, T.; Rougée, M.; Hélène, C.; Lehn, J.-M. *Biochemistry* **1989**, *28*, 3227. (b) Slama-Schwok, A.; Rougée, M.; Ibanez, V.; Geacintov, N. E.; Montenay-Garestier, T.; Lehn, J.-M.; Hélène, C. *Biochemistry* **1989**, *28*, 3234. (c) Brun, A. M.; Harriman, A. *J. Am. Chem. Soc.* **1991**, *113*, 8153. (d) Basuray, A. N.; Jacquot de Rouville, H.-P.; Hartlieb, K. J.; Kikuchi, T.; Strutt, N. L.; Bruns, C. J.; Ambrogio, M. W.; Avestro, A.-J.; Schneckeli, S. T.; Fahrenbach, A. C.; Stoddart, J. F. *Angew. Chem., Int. Ed.* **2012**, *51*, 11872. (e) Basuray, A. N.; de Rouville, H.-P. J.; Hartlieb, K. J.; Fahrenbach, A. C.; Stoddart, J. F. *Asian J. Chem.* **2013**, *8*, 524. (f) Hartlieb, K. J.; Basuray, A. N.; Ke, C.; Sarjeant, A. A.; Jacquot de Rouville, H.-P.; Kikuchi, T.; Forgan, R. S.; Kurutz, J. W.; Stoddart, J. F. *Asian J. Org. Chem.* **2013**, *2*, 225. (g) Sampath, S.; Basuray, A. N.; Hartlieb, K. J.; Aytun, T.; Stupp, S. I.; Stoddart, J. F. *Adv. Mater.* **2013**, *25*, 2740. (h) Hartlieb, K. J.; Witus, L. S.; Ferris, D. P.; Basuray, A. N.; Algaradah, M. M.; Sarjeant, A. A.; Stern, C. L.; Nassar, M. S.; Botros, Y. Y.; Stoddart, J. F. *ACS Nano* **2015**, *9*, 1461. (i) Hou, X.; Ke, C.; Bruns, C. J.; McGonigal, P. R.; Pettman, R. B.; Stoddart, J. F. *Nature Commun.* **2015**, *6*, Article 6884.

- 1  
2  
3  
4  
5  
6  
7  
8  
9  
10  
11  
12  
13  
14  
15  
16  
17  
18  
19  
20  
21  
22  
23  
24  
25  
26  
27  
28  
29  
30  
31  
32  
33  
34  
35  
36  
37  
38  
39  
40  
41  
42  
43  
44  
45  
46  
47  
48  
49  
50  
51  
52  
53  
54  
55  
56  
57  
58  
59  
60
11. Functionalized PDIs tend to exhibit increased solubilities in organic solvents. Although examples of the incorporation of a PDI unit, modified at its bay position (Figure 1a), into symmetrical cyclophanes have been report by the Würthner group, functionalization at the bay positions might interfere with binding of guests by the cyclophane, while functionalization at the imide positions with alkyl groups may not be appropriate in a robust cyclophane architecture. See (a) Schlosser, F.; Moos, M.; Lambert, C.; Würthner, F. *Adv. Mater.* **2013**, 25, 410. (b) Spenst, P.; Würthner, F. *Angew. Chem., Int. Ed.* **2015**, 54, 10165.
  12. Hunter, C. A.; Sanders, J. K. M. *J. Am. Chem. Soc.* **1990**, 112, 5525.
  13. In most cases, the geometry of molecules is not necessarily the same in solution as in the solid-sate because of thermal and environmental disorder. In the case of the **DAPPBox**<sup>4+</sup>, however, this potential mismatching of distances should be much less of an issue as a consequence of the rigidity of the cyclophane, where the range of accessible geometries in solution is quite limited. Therefore, it is not unreasonable to consider the crystal structure as an "equilibrium geometry" about which the solution-state geometry will fluctuate, as a result of both solvent and thermal fluctuations.
  14. Barnes, J. C.; Fahrenbach, A. C.; Dyar, S. M.; Frasconi, M.; Giesener, M. A.; Zhu, Z.; Liu, Z.; Hartlieb, K. J.; Carmieli, R.; Wasielewski, M. R.; Stoddart, J. F. *Proc. Natl. Acad. Sci. USA* **2012**, 109, 11546.
  15. Takahashi, M.; Suzuki, Y.; Ichihashi, Y.; Yamashita, M.; Kawai, H. *Tetrahedron Lett.* **2007**, 48, 357.
  16. Zheng, J.; Li, Y.; Sun, Y.; Yang, Y.; Ding, Y.; Lin, Y.; Yang, W. *ACS Appl. Mater. Interfaces* **2015**, 7, 7241.
  17. Dolomanov, O. V.; Bourhis, L. J.; Gildea, R. J.; Howard, J. A. K.; Puschmann, H. *J. Appl. Crystallogr.* **2009**, 42, 339.
  18. Sheldrick, G. *Acta Crystallographica Section C* **2015**, 71, 3.
  19. Dixon, J. M.; Taniguchi, M.; Lindsey, J. S. *Photochem. Photobiol.* **2005**, 81, 212.



## Captions to Schemes and Figures

**Scheme 1. The Synthesis of DAPPBox•4PF<sub>6</sub>.**

**Scheme 2. Schematic Representation of the Photodriven Charge Redistribution Yielding the DAPP<sup>3+</sup> – ExBIPY<sup>•+</sup> Radical Ion-Pair in DAPPBox<sup>4+</sup>.**

**Figure 1.** Structural formulas of (a) **PDI**, (b) **ExBIPY<sup>2+</sup>**, (c) **DAPP<sup>2+</sup>**, and (d) **DAPPBox<sup>4+</sup>**.

**Figure 2.** <sup>1</sup>H NMR Spectra of **4•2PF<sub>6</sub>** and **DAPPBox•4PF<sub>6</sub>** (500 MHz, CD<sub>3</sub>CN, 298K).

**Figure 3.** Solid-state (super)structure of the **DAPPBox<sup>4+</sup>** obtained from X-ray crystallography on single crystals of **DAPPBox•4TFA**. (a) Perspective view of the **DAPPBox<sup>4+</sup>** as a stick representation with the corresponding semi-transparent space-filling representations superimposed upon it. (b) Plan view of stick representation **DAPPBox<sup>4+</sup>** ring showing distances and torsional angles associated with the ring's geometry. (c) Solid-state superstructure of **DAPPBox<sup>4+</sup>** reveals a herring-bone type of packing and two types of  $\pi\cdots\pi$  interactions<sup>12</sup> as labeled above results in flatter features for the **ExBIPY<sup>2+</sup>** unit (smaller torsional angle between adjacent pyridinium rings, ~17° and ~20°, respectively) in **DAPPBox<sup>4+</sup>**, compared<sup>8a</sup> (~30°) with its **ExBox<sup>4+</sup>** analog. (d) Perspective view of the superstructure of **DAPPBox<sup>4+</sup>** demonstrating the partial overlap between the **ExBIPY<sup>2+</sup>** and **DAPP<sup>2+</sup>** units in adjacent cyclophanes, probably resulting from the balance between Coulombic repulsions and the maximization of  $\pi$ -overlap.

**Figure 4.** (a) Structural formulas of **Me-ExBIPY<sup>2+</sup>** and **Me-DAPP<sup>2+</sup>**, which were used as reference compounds for the EnT process within **DAPPBox<sup>4+</sup>**. (b) Structural formulas of **Bn-ExBIPY<sup>2+</sup>** and **Bn-DAPP<sup>2+</sup>**, which were used as reference compounds for the ET process within **DAPPBox<sup>4+</sup>**.

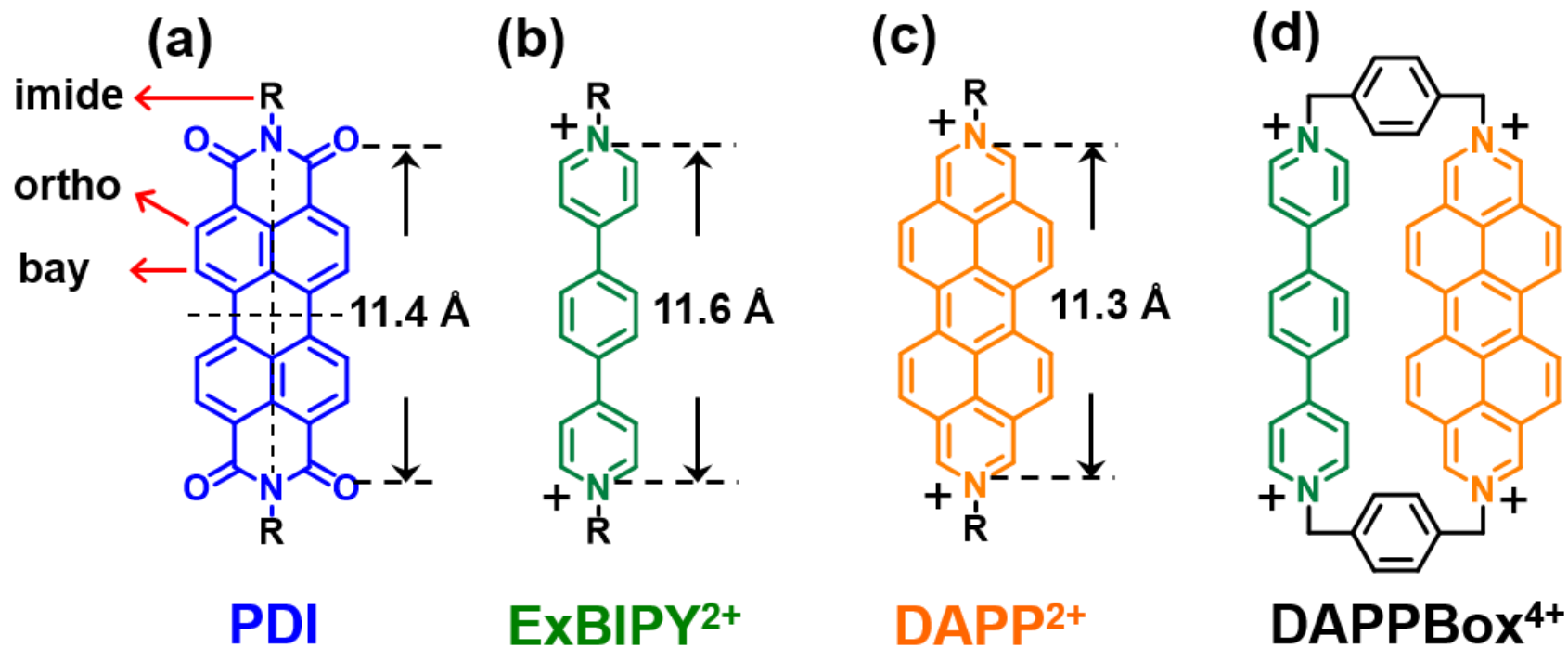
**Figure 5.** Absorption spectra of **DAPPBox**<sup>4+</sup>, **Me-ExBIPY**<sup>2+</sup> and **Me-DAPP**<sup>2+</sup> in MeCN at room temperature.

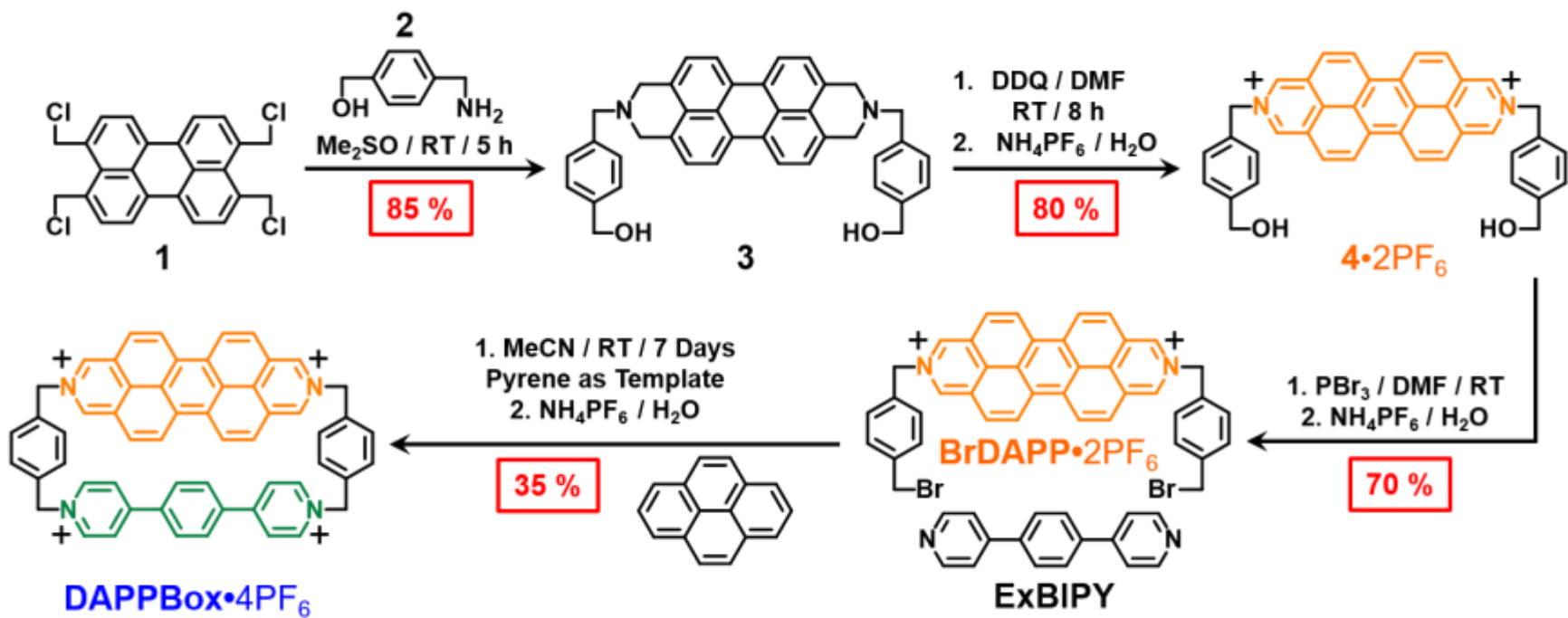
**Figure 6.** Visible and NIR (a) fsTA, 330 nm excitation, (b) fsTA, 505 nm excitation spectra of **DAPPBox**<sup>4+</sup> in MeCN at room temperature. In Figure 6a, the spectra beyond 850 nm are scaled by a factor of two for clarity.

**Figure 7.** (a) Energy transfer process within **DAPPBox**<sup>4+</sup>. (b) Emission spectra of **DAPPBox**<sup>4+</sup>, **Me-ExBIPY**<sup>2+</sup>, **Me-DAPP**<sup>2+</sup> and a physical mixture of **Me-ExBIPY**<sup>2+</sup> and **Me-DAPP**<sup>2+</sup> in MeCN upon excitation at 339 nm, 1.6  $\mu$ M. (c) Normalized spectra showing the overlap between emission of the **Me-ExBIPY**<sup>2+</sup> and the absorption of the **Me-DAPP**<sup>2+</sup>. (d) The overlap between excitation spectrum ( $\lambda_{\text{em}} = 554$  nm) and the UV/Vis absorption spectrum of **DAPPBox**<sup>4+</sup>.

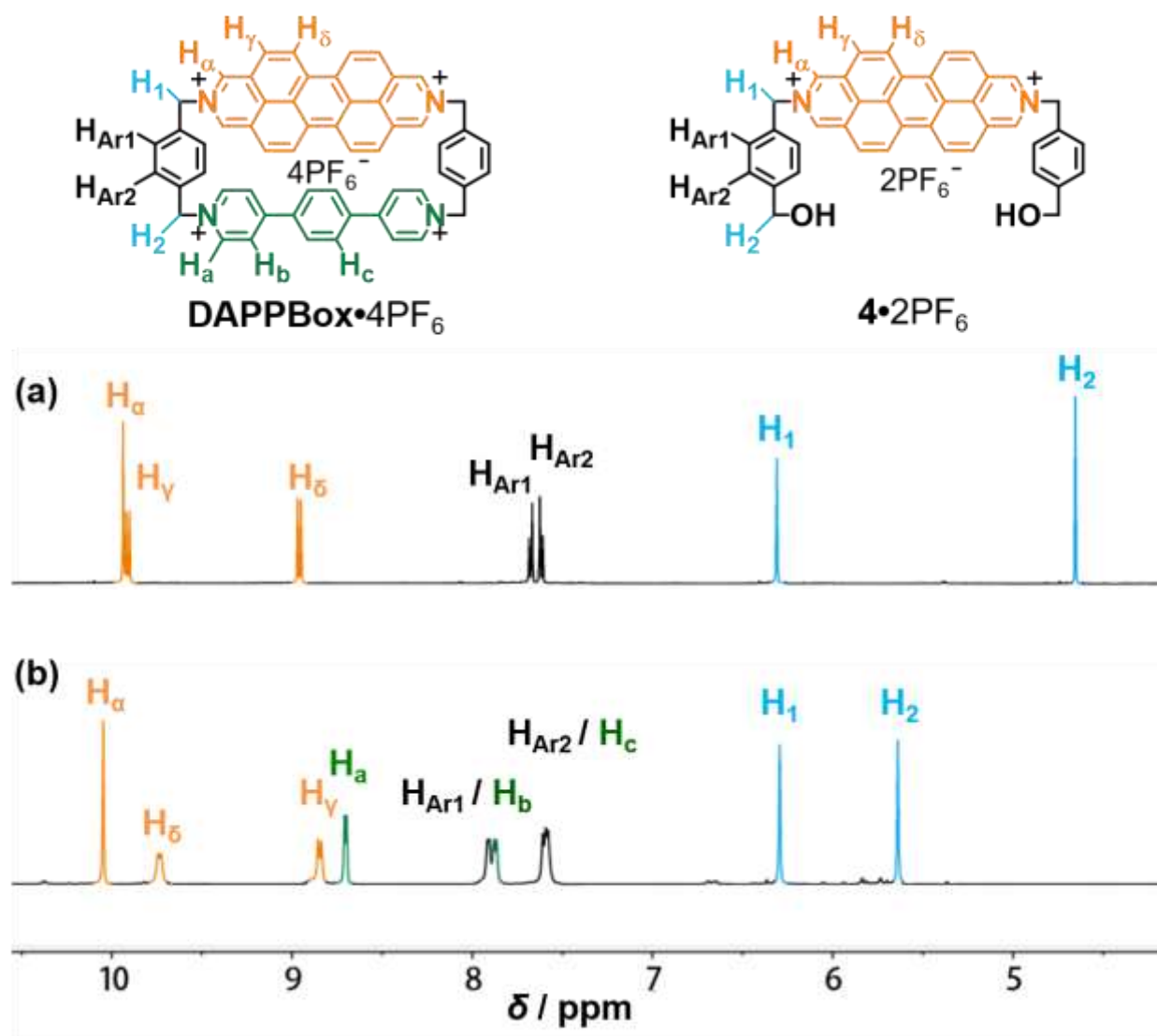
**Figure 8.** Kinetic decays at 495 nm for (a) **DAPPBox**<sup>4+</sup> (black), **Bn-DAPP**<sup>2+</sup> (red), and **Bn-ExBIPY**<sup>2+</sup> (green) following 60 fs, 330 nm (1  $\mu$ J/pulse) excitation and (b) **DAPPBox**<sup>4+</sup> excited at 330 nm (black) and 414 nm (blue). Only the first 10 ps are shown in order to highlight the ultrafast decay of the **DAPPBox**<sup>4+</sup> trace, which is not present in the reference compounds. The fit of the full **DAPPBox**<sup>4+</sup> kinetic decay is also shown; nanosecond lifetimes obtained from nsTA spectroscopy (Figure S35 to 37). All traces were normalized to their respective values at 8 ps.

**Figure 9.** Schematic of the excited-state relaxation pathways in **DAPPBox**<sup>4+</sup> at different excitation wavelengths (IC = internal conversion; ISC = intersystem crossing; f = fluorescence; FET = forward electron transfer; BET = back electron transfer; EnT = energy transfer). Dashed arrows indicated radiative transitions. Red X's indicated kinetically unfavorable processes.

**Figure 1**



Scheme 1

**Figure 2**

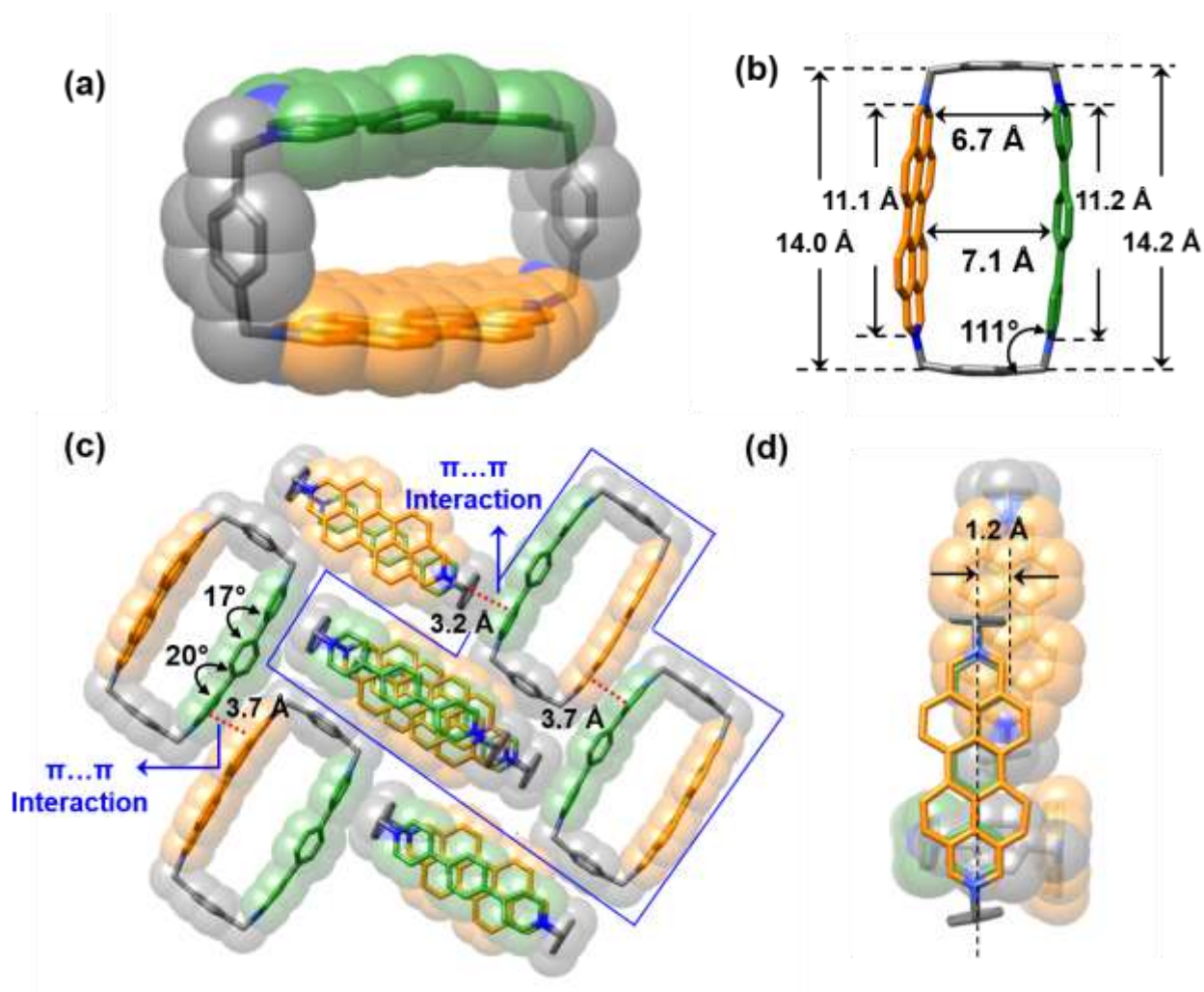
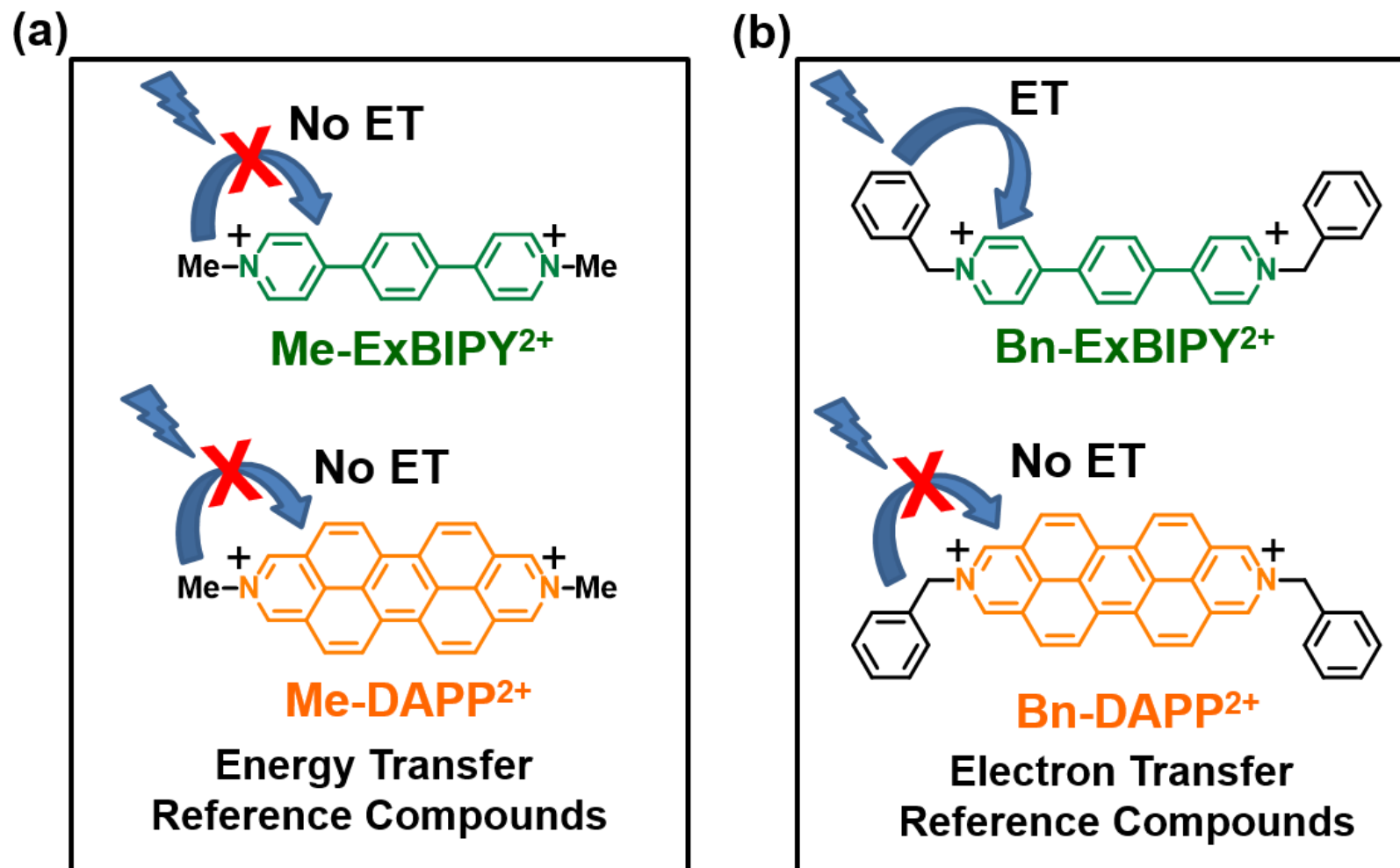


Figure 3

**Figure 4**

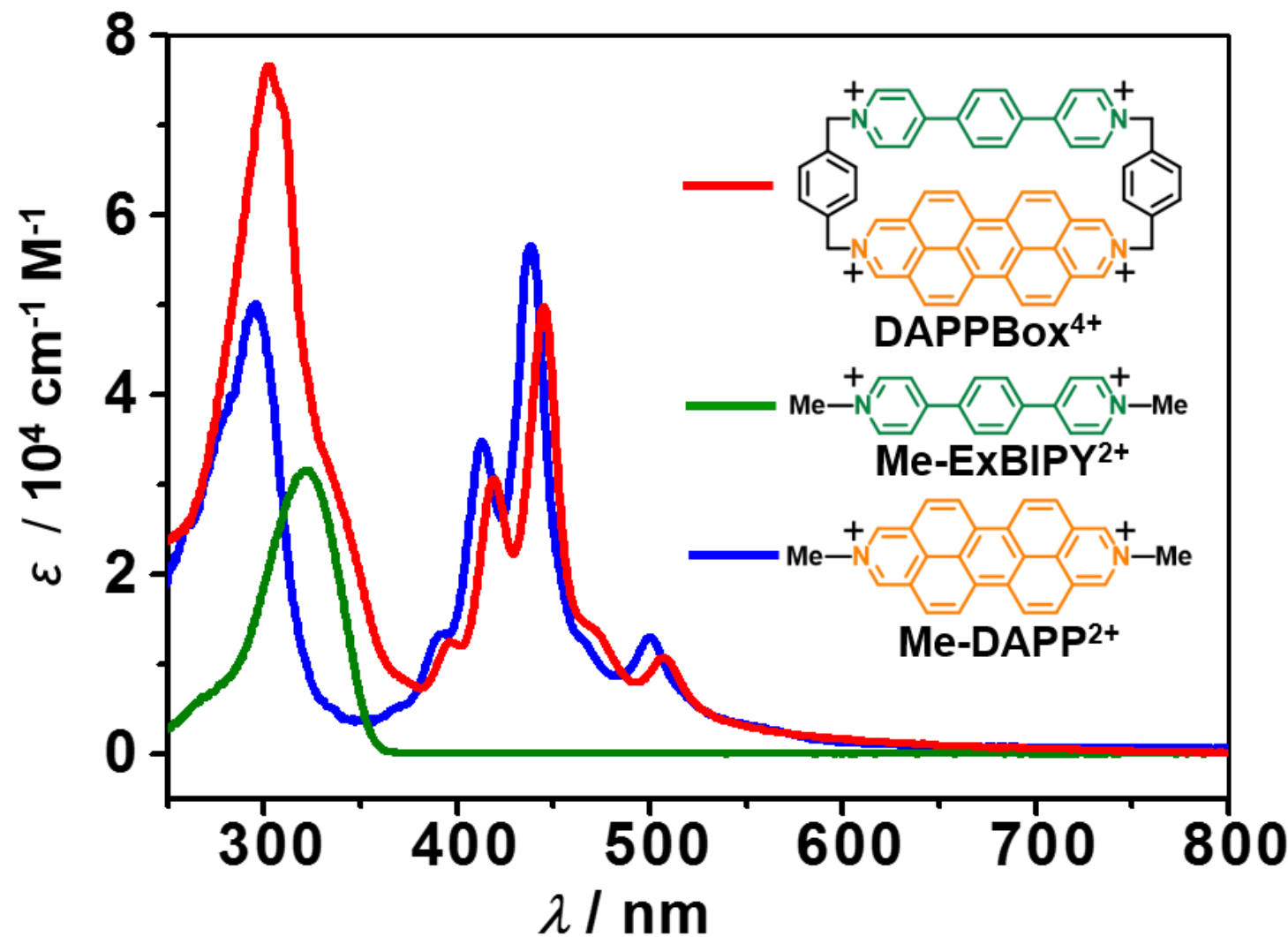
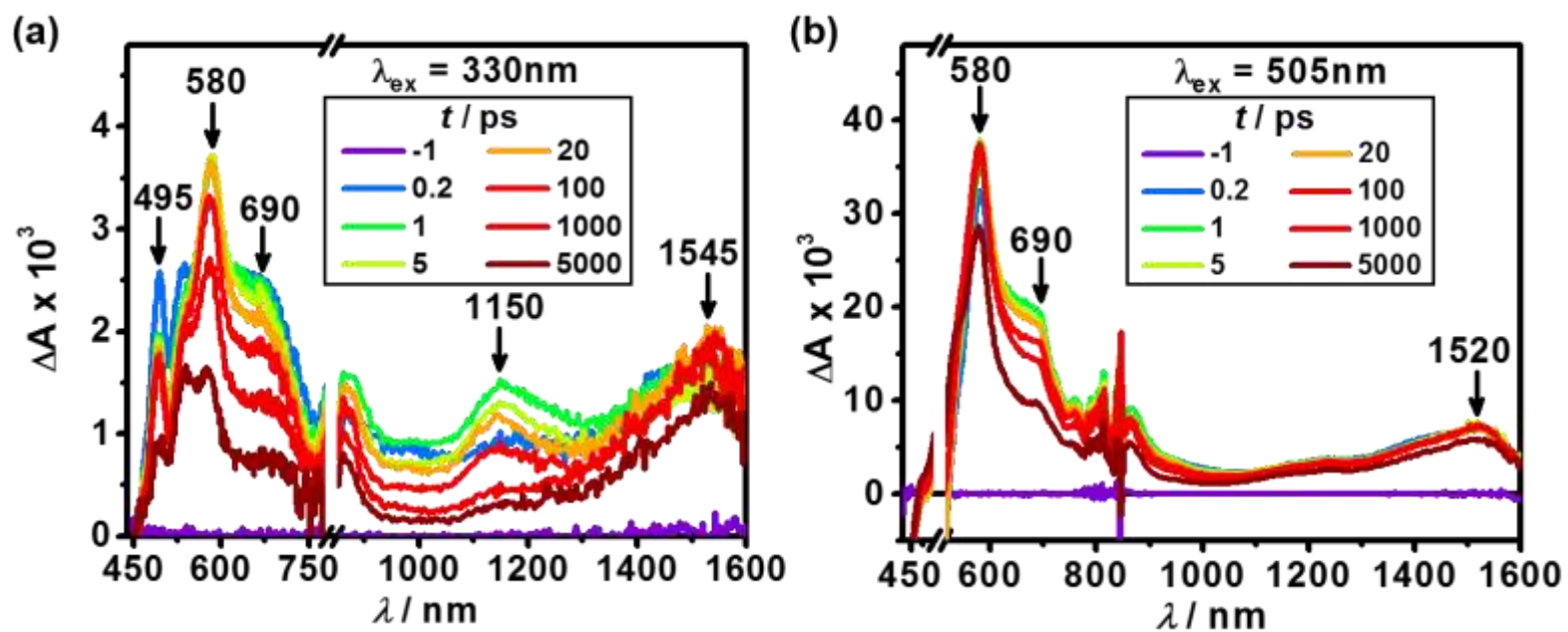


Figure 5



**Figure 6**

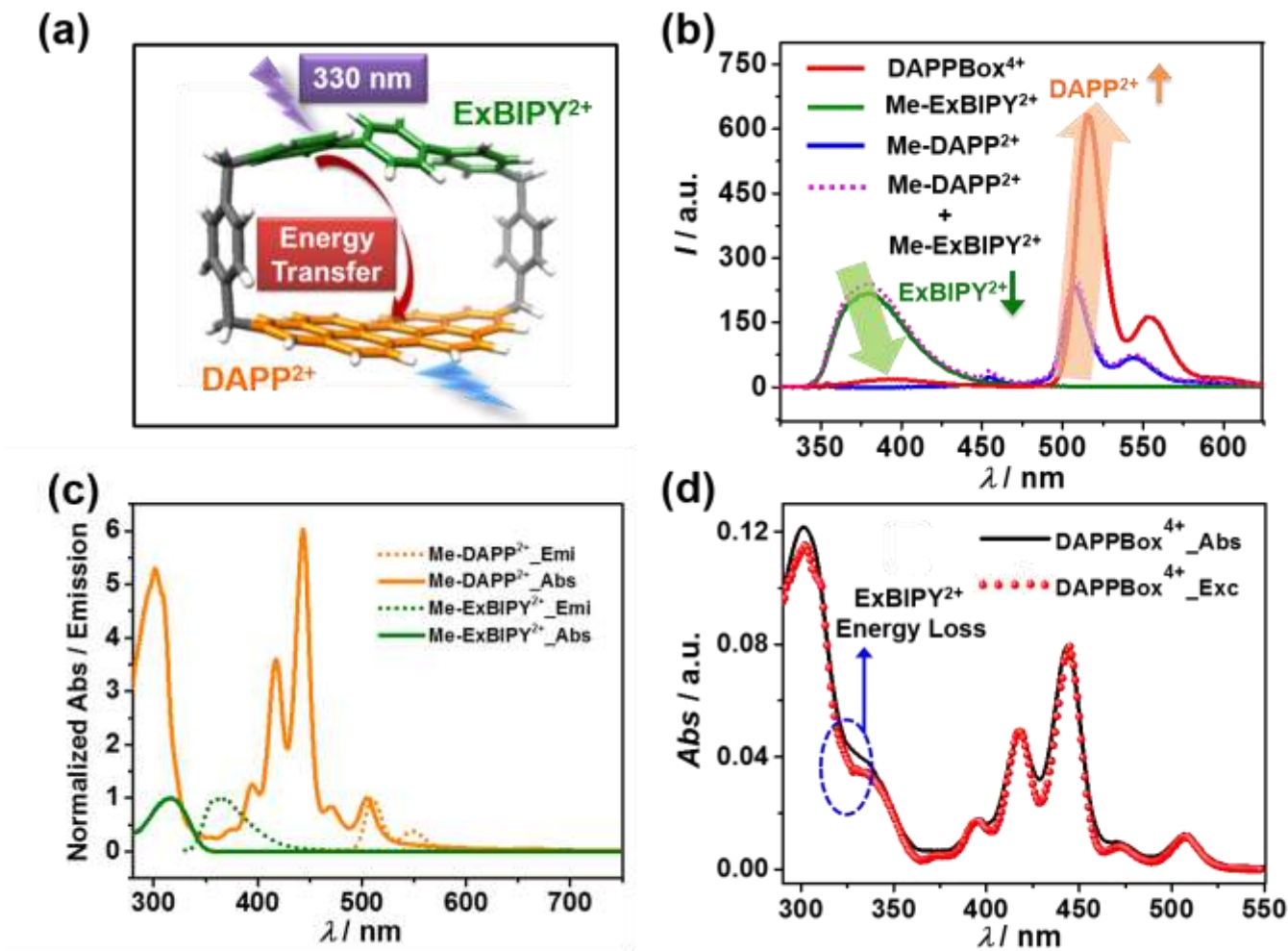


Figure 7

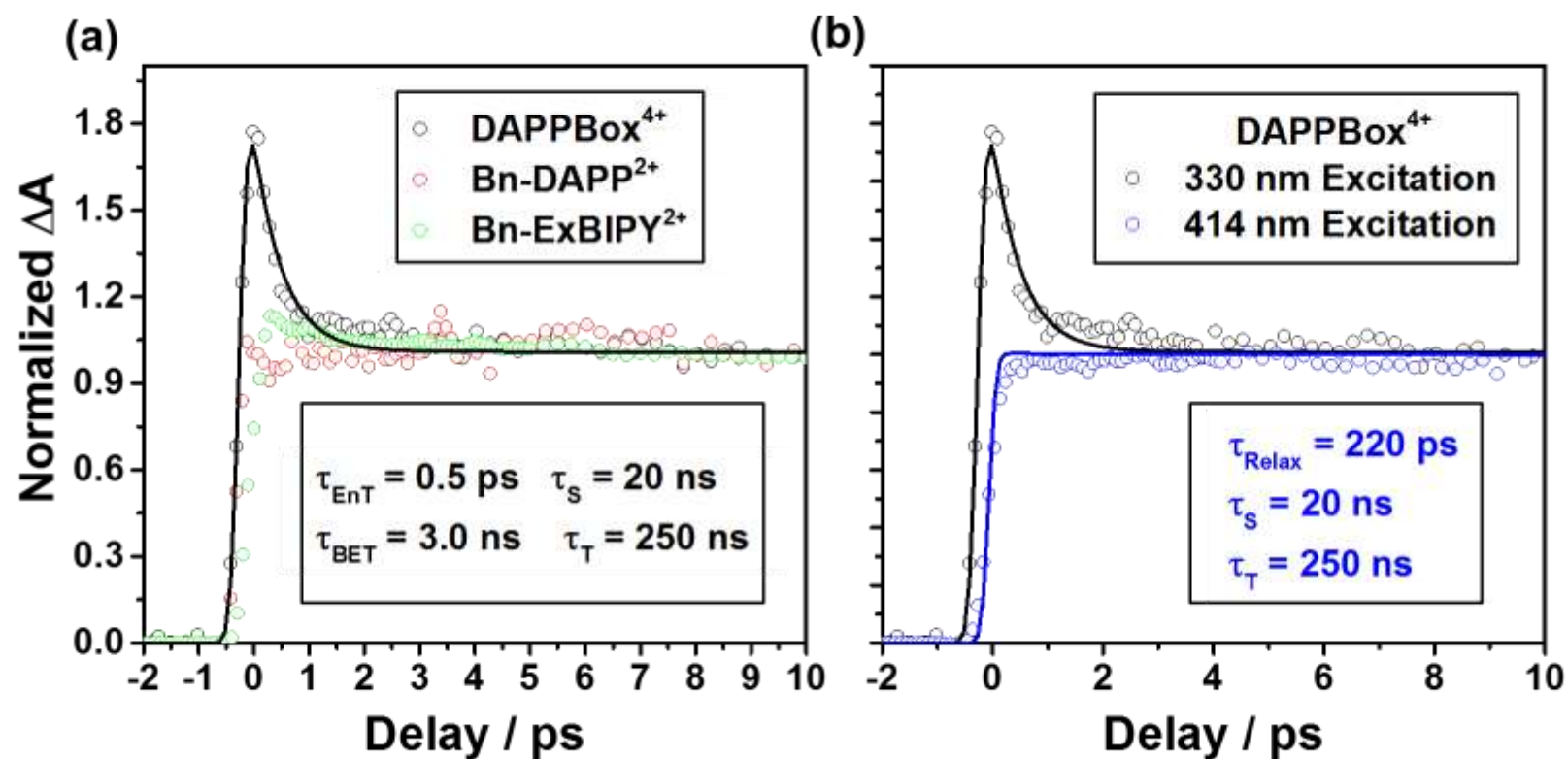


Figure 8

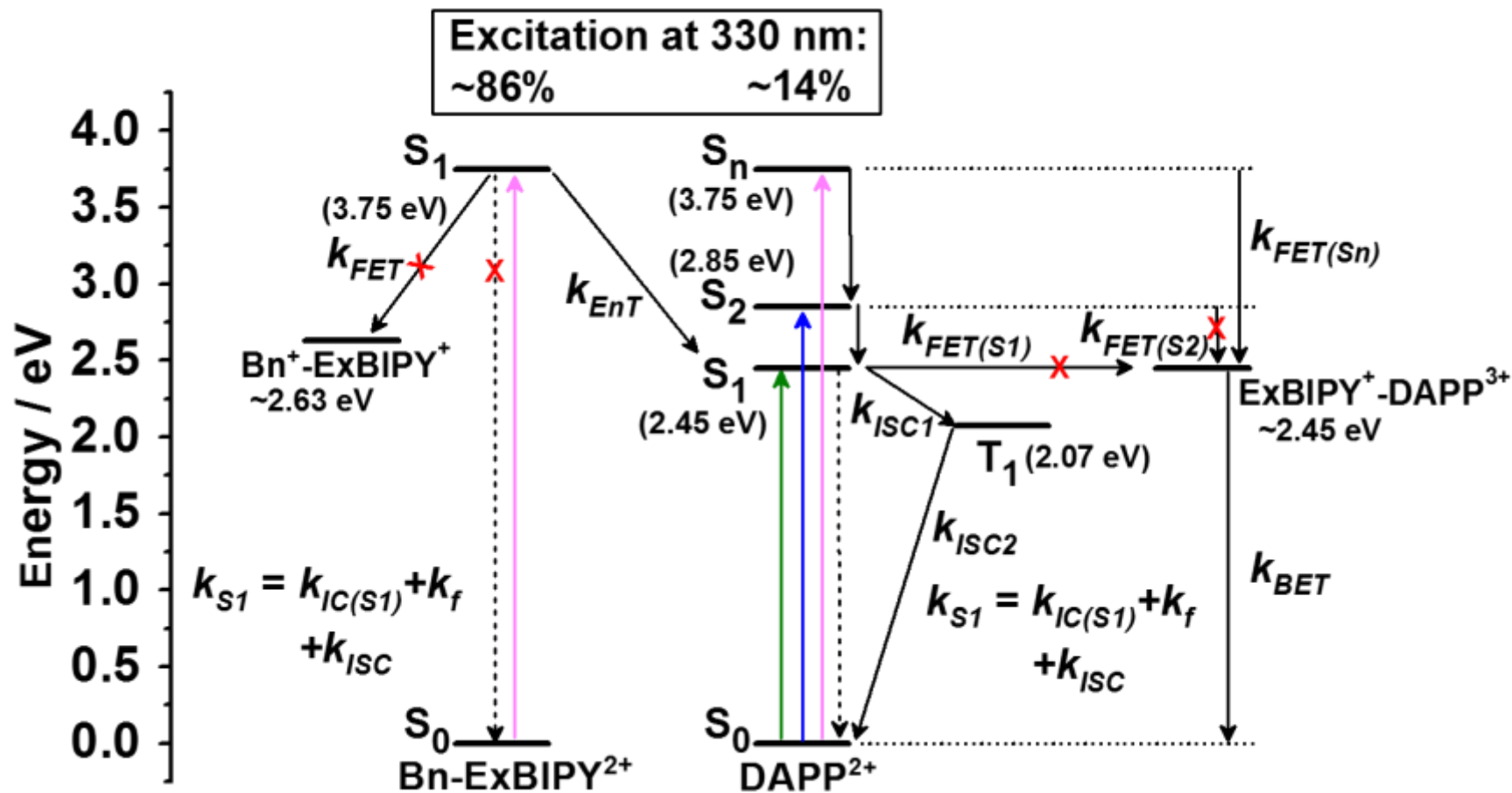
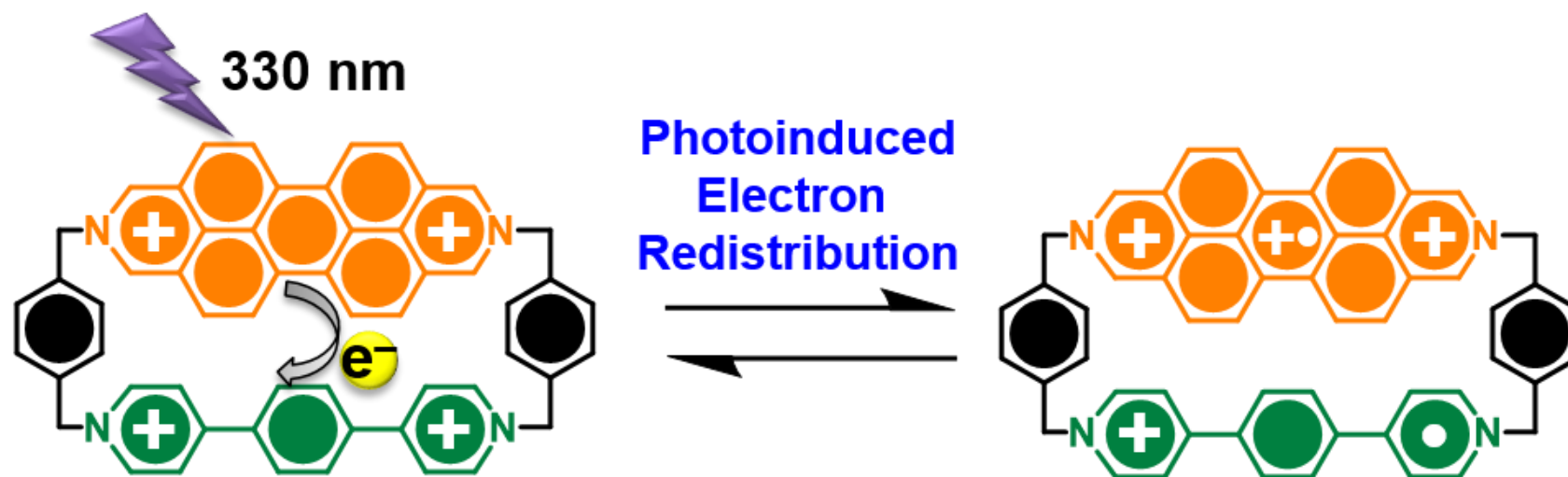


Figure 9



## Scheme 2

Table 1. Photophysical Properties of the Reference Compounds and DAPPBox<sup>4+</sup>

Compound	<sup>a</sup> $\lambda_{\text{abs}}$ (nm) / $\epsilon_{\text{max}}$ (10 <sup>4</sup> M <sup>-1</sup> cm <sup>-1</sup> )	<sup>a</sup> $\lambda_{\text{ems}}$ (nm)	<sup>b</sup> $\tau$ (ns) / <sup>a</sup> $\lambda_{\text{exc}}$ (nm)	<sup>c</sup> $\Phi_{\text{ems}}$
Me-ExBIPY <sup>2+</sup>	323 (3.15)	364	1.56 (330)	0.69
Me-DAPP <sup>2+</sup>	438 (5.66)	505	17.6 (375)	0.66
Bn-ExBIPY <sup>2+</sup>	321 (2.31)	378	0.062 (330)	0.04
Bn-DAPP <sup>2+</sup>	443 (5.74)	509	19.8 (375)	0.60
DAPPBox <sup>4+</sup>	442 (4.98)	520	19.5 (374)	0.39

<sup>a</sup> $\lambda_{\text{abs}}$  /  $\lambda_{\text{ems}}$  /  $\lambda_{\text{exc}}$ : maximum absorption, emission and excitation wavelengths; <sup>b</sup> $\tau$ : fluorescence lifetime;

<sup>c</sup> $\Phi_{\text{ems}}$ : fluorescence quantum yield.

# For Table of Contents Only

